APPENDICES

APPENDIX A: FITTING FT-IR DATA

INTRODUCTION

According to the literature consumption of the epoxy in the cure process is best described by the equation [1]:

$$r = d\alpha / dt = \left(k_1 + k_2.\alpha^m\right)(1-\alpha)^n$$

Equation 1

where α is the degree of conversion and k_1 and k_2 are apparent rate constants, r is the reaction rate defined $d\alpha / dt$ and m and n the kinetic exponents of the reaction.

As an illustration of the fitting procedure, PR55 cured at 35°C has been taken as the data set that provides the most complete curve resembling that predicted by an equation of the form Equation 1, as shown in Figure 1. A Mathcad programme was written to simulate Equation 1 and allow the constants to be adjusted to achieve a fit of the data.

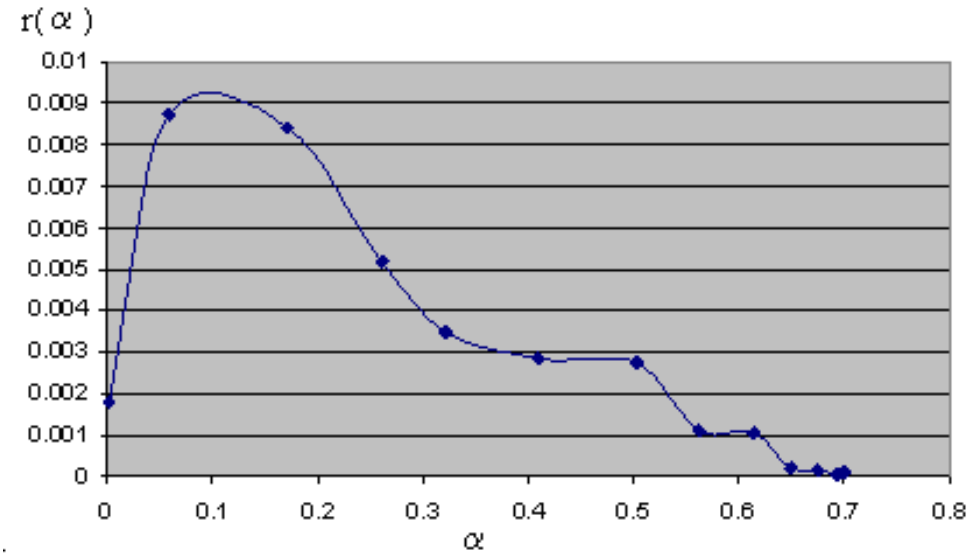

Figure 1. Plot of the function r(α) against α for PR55 cured at 35°C.

The fit for PR55 cured at 35°C is shown in Figure 2 with k_1 = 8 x 10^{-3} s^{-1}; k_2 = 8 x 10^{-3} s^{-1}; m=0.5 and n= 3.3. The fit is sensitive to the value of k_2, with the amplitude of the peak scaling with the magnitude of the constant. The creation of the peak is dependent the value of k_1. The slope is very sensitive to the value of n and reflects the contribution of the autocatalytic reaction in the total process. The fit between the experimental and the theoretical is surprisingly good and confirms previous authors

assumptions that the epoxy cure data is best fitted by a function of the form of Equation 1. A manual fit of the data was attempted using the first data points - collected at short times it has a low level of precision and produced fits of the data which were unacceptable.

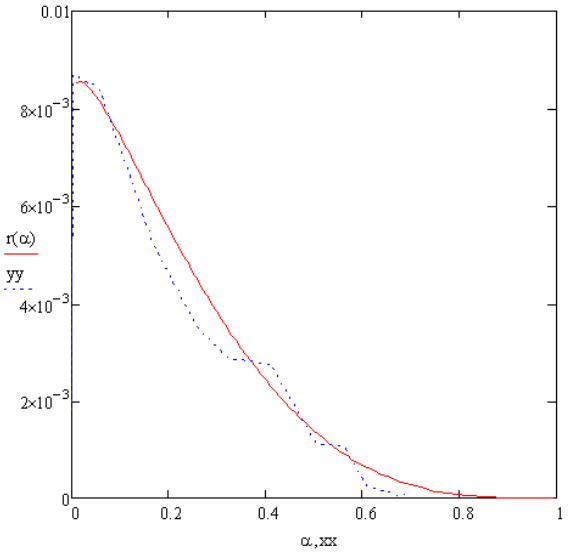

Figure 2. Comparison of theory based on Equation 1 and the experimental function (Figure 1) for PR55 at 35°C.

PR55

The r(α) versus α function for PR55 at 30°C is shown in Figure 3. As previously described the data set was fitted to Equation 1 and the results are shown in Figure 4. Fitting parameters from the comparison were k_1 = 1 x 10^{-3} s^{-1}; k_2 = 1.3 x 10^{-2} s^{-1}; m = 0.5 and n=3.0. The value of m is unchanged and the value of n has been reduced to 3.0 compared to the results for 30°C. In this case the values of k_1 and k_2 are very different which is in contrast to the values obtained when fitting the data at 35°C.

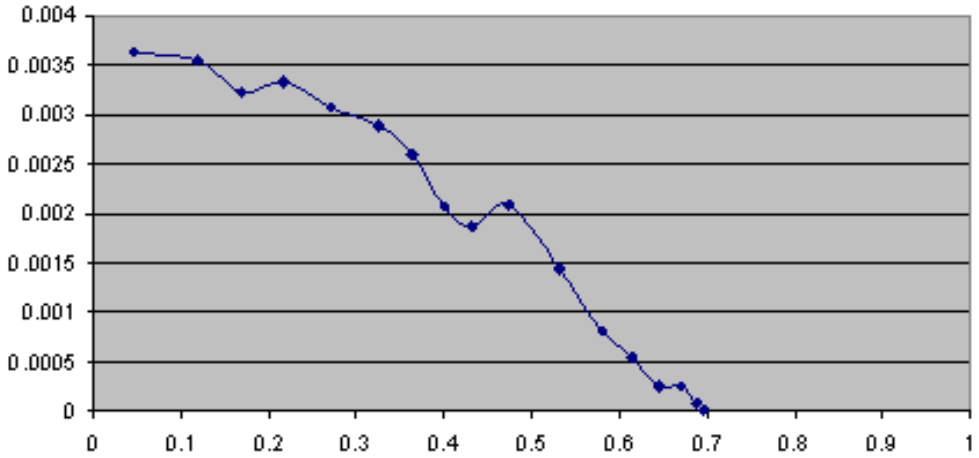

Figure 3. Plot of the function r(α) against α for PR55 cured at 30^0C.

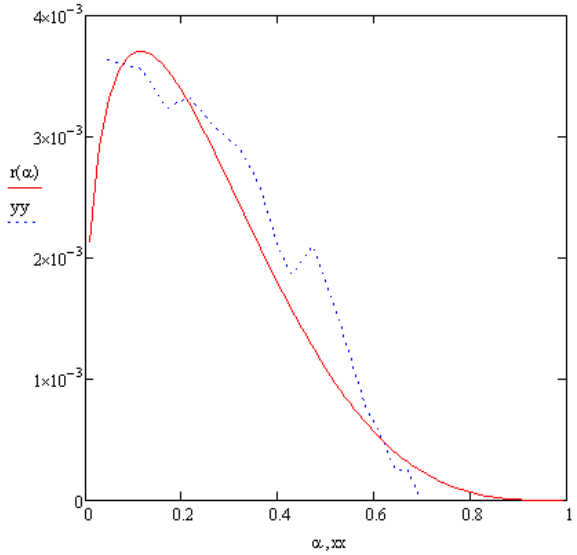

Figure 4. Comparison of theory based on Equation 1 and the experimental function (Figure 3) for PR55 at 30°C.

The function r(α) as a function of α for that data collected at 25°C is shown in Figure 5, with the comparison given in Figure 6. The values of the fitting parameters are k_1 = 1 x 10^{-3} s^{-1}; k_2 = 2.3 10^{-3} s^{-1}; m= 0.05 and n = 2.0. The surprising observation is that the value of m had to be reduced significantly to a very low value of 0.05. The values of k_1 and k_2 are relatively close.

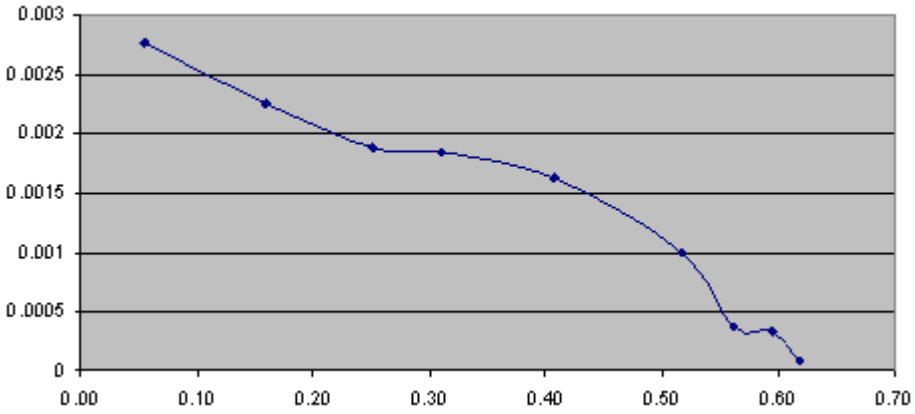

Figure 5. Plot of the function r(α) against α for PR55 cured at 25°C.

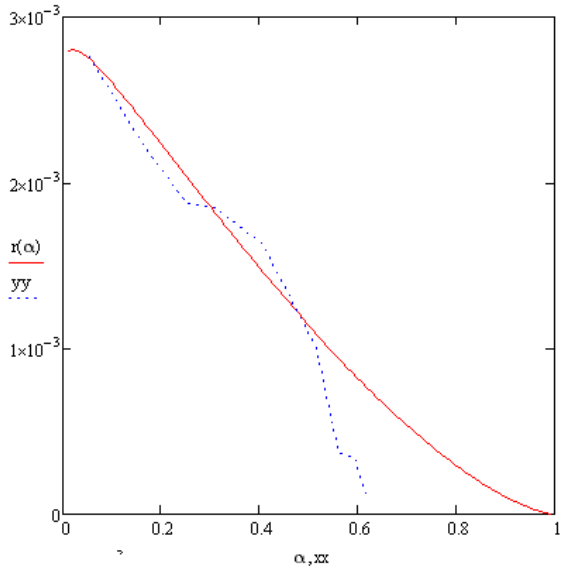

Figure 6. Comparison of theory based on Equation 1 and the experimental function (Figure 5) for PR55 at 25°C.

For the PR55 system Equation 1 can be used to fit the data at low degrees of conversion but is not able to fit the data at high degrees of conversion where diffusion and other effects would be expected to influence the rates of the reaction.

Strathclyde Model System

The cure using TETA was selected as the model system for the Strathclyde study. The data obtained are summarised below, Figure 7. The 30°C graph contains both the original and the repeat measurements.

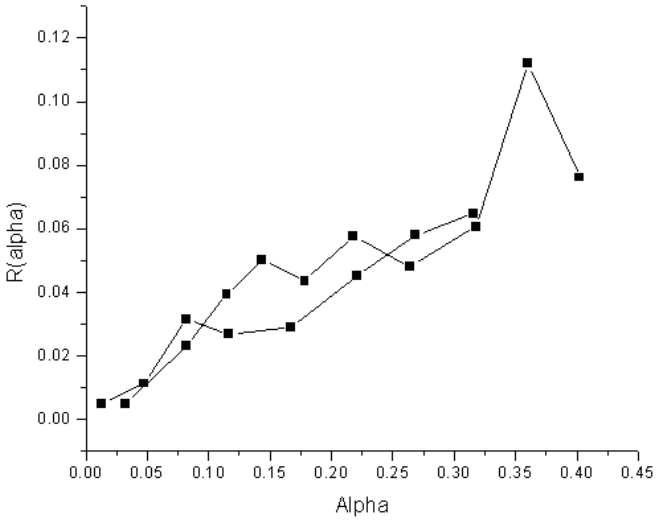

Figure 7. Plot of the function r(α) against α for the Strathclyde model system cured at 30°C.

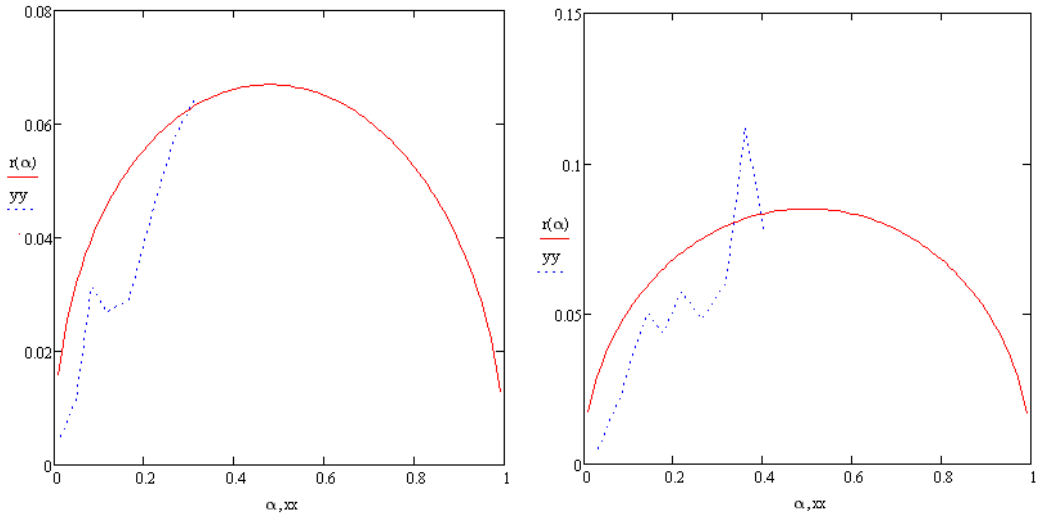

Figure 8. Comparison of theory based on Equation 1 and the experimental function (Figure 7) for the Strathclyde model system at 30°C for both the original (LHS) and repeat (RHS) data sets.

The fitting parameters obtained from Figure 8 are $k_1 = 1 \times 10^{-4}\ s^{-1}$; $k_2 = 15 \times 10^{-2}\ s^{-1}$; m = 0.5 and n = 0.48 for the original data, and are $k_1 = 0.1 \times 10^{-4}\ s^{-1}$, $k_2 = 17 \times 10^{-2}\ s^{-1}$, m = 0.5 and n = 0.5 for the repeat data set. In the case of the fit for the repeat data set the peak is ignored as this corresponds to long time data and is probably in error as a consequence of instability in the FT-IR.

The data set obtained for the Strathclyde model system at 35°C is summarised in Figure 9. The fitting parameters obtained from Figure 10 are $k_1 = 0.01 \times 10^{-2}\ s^{-1}$, k_2

= 21 x 10^{-2} s^{-1}, m = 0.8 and n = 1. for the original set and are k_1 = 0.1 x 10^{-2} s^{-1}, k_2 = 41 x 10^{-2} s^{-1}, m = 1.5 and n = 0.4 for the repeat. In the case of the fit for the original data, the high values were ignored. The fits are very different for the two sets of data and the most convincing was the repeat set.

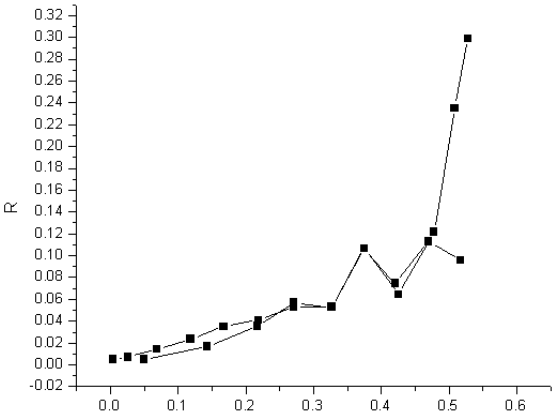

Figure 9. Plot of the function r(α) against α for the Strathclyde model system cured at 35°C.

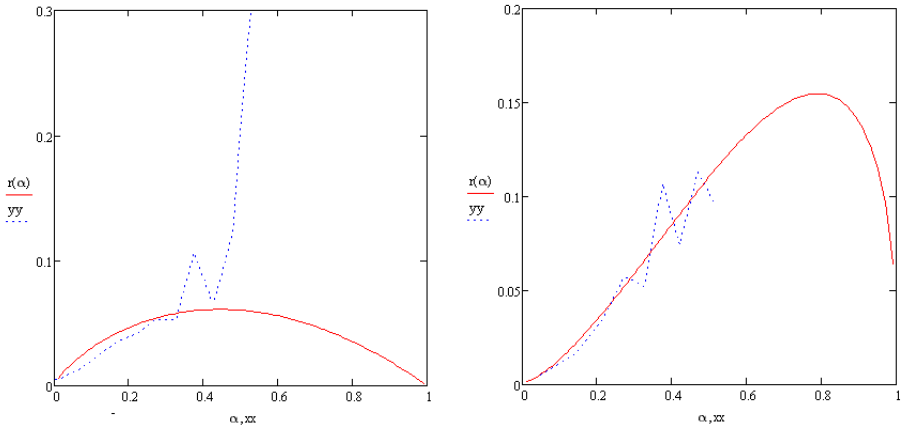

Figure 10. Comparison of theory based on Equation 1 and the experimental function Figure 9 for the Strathclyde model system at 35°C.

The data set obtained for the Strathclyde model system at 40°C is summarised in Figure 11. The fitting parameters obtained from Figure 12 are k_1 = 0.1 x 10^{-2} s^{-1}, k_2 = 41 x 10^{-2} s^{-1}, m = 1.5 and n = 0.4 for the original set and are are k_1 = 0.05 x 10^{-2} s^{-1}, k_2 = 41 x 10^{-2} s^{-1}, m = 1.5 and n = 0.5 for the repeat set.

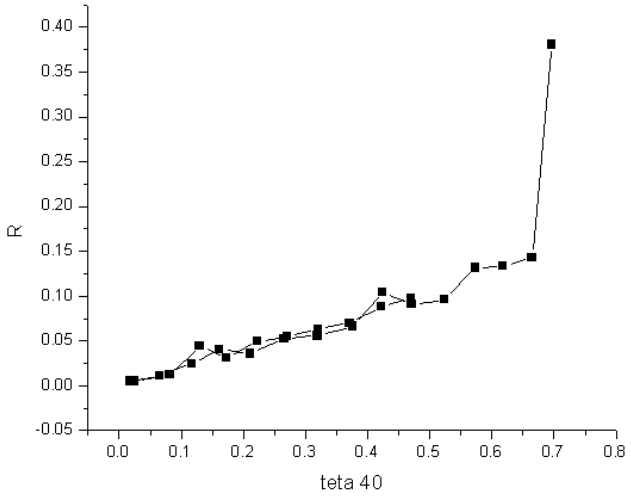

Figure 11. Plot of the function r(α) against α for the Strathclyde model system cured at 40°C.

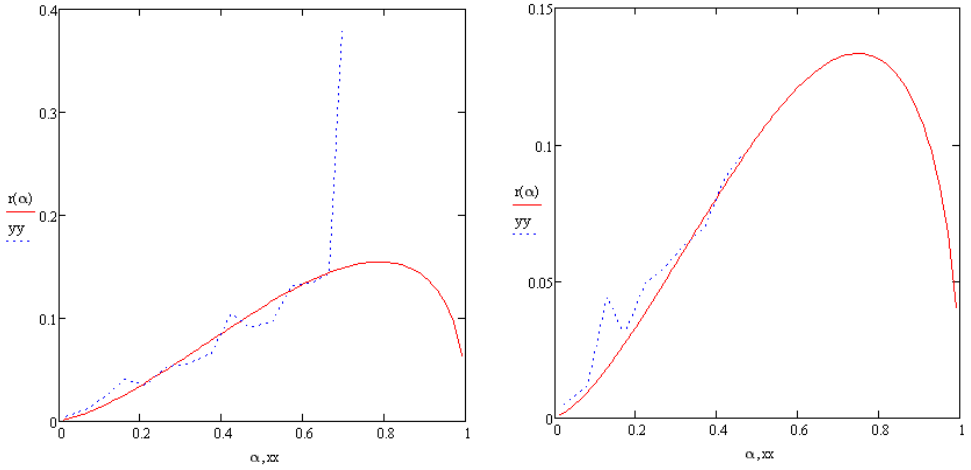

Figure 12. Comparison of theory based on Equation 1 and the experimental function Figure 11 for the Strathclyde model system at 40°C.

The data set obtained for the Strathclyde model system at 45°C is summarised in Figure 13. The last point in the original set (at ca. 0.5, 0.02) has been ignored in the analysis.

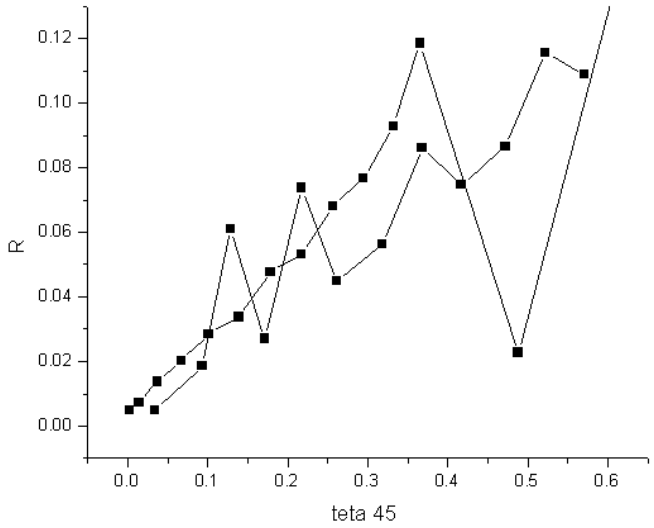

Figure 13. Plot of the function r(α) against α for the Strathclyde model system cured at 45°C.

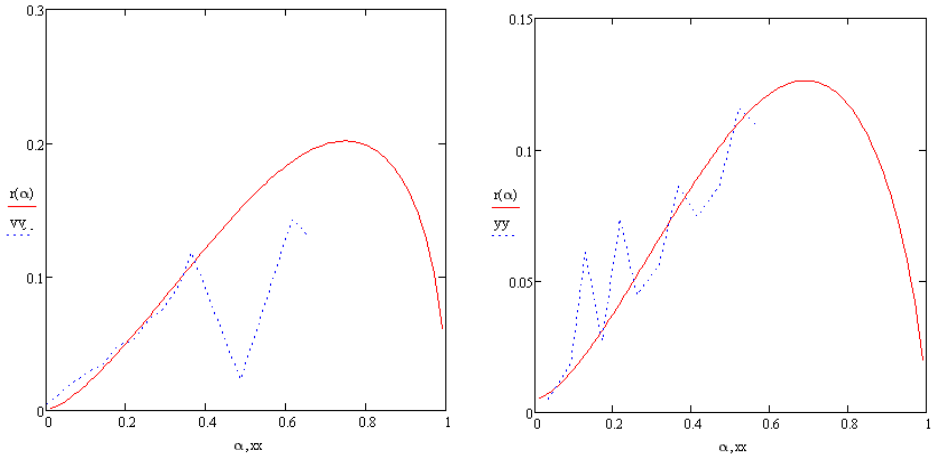

Figure 14. Comparison of theory based on Equation 1 and the experimental function Figure 13 for the Strathclyde model system at 45°C.

The fitting parameters obtained from Figure 14 are $k_1 = 0.05 \times 10^{-2}$ s^{-1}, $k_2 = 62 \times 10^{-2}$ s^{-1}, m = 1.5 and n = 0.5 for the original set and are $k_1 = 0.5 \times 10^{-2}$ s^{-1}, $k_2 = 51 \times 10^{-2}$ s^{-1}, m = 1.6 and n = 0.7 for the repeat set. There were problems with fitting both sets of data as the scatter in the function r(α) in both cases was large.

The data set obtained for the Strathclyde model system at 50°C is summarised in Figure 15 – a repeat set was not measured.

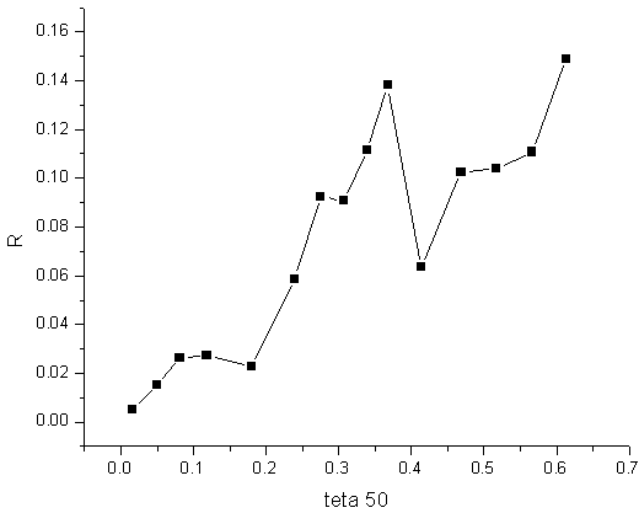

Figure 15. Plot of the function r(α) against α for the Strathclyde model system cured at 50°C.

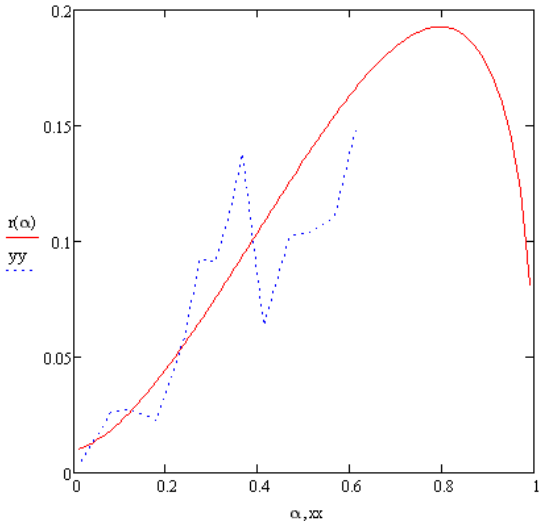

Figure 16. Comparison of theory based on Equation 1 and the experimental function Figure 15 for the Strathclyde model system at 50°C.

The fitting parameters obtained from Figure 16 are $k_1 = 1 \times 10^{-2}\ s^{-1}$, $k_2 = 51 \times 10^{-2}\ s^{-1}$, m = 1.6 and n = 0.4. There is a high degree of scattering in the data which raises questions about the validity of the data obtained from the fits.

Shared Model System

This system was more difficult to obtain a satisfactory fit of the data. The experimental data for 70°C is shown in Figure 17, and the fitting of the data in Figure

18. The fitting parameters obtained are k_1 = 11 x 10^{-2} s^{-1}, k_2 = 180 x 10^{-2} s^{-1}, m = 0.5 and n = 6.

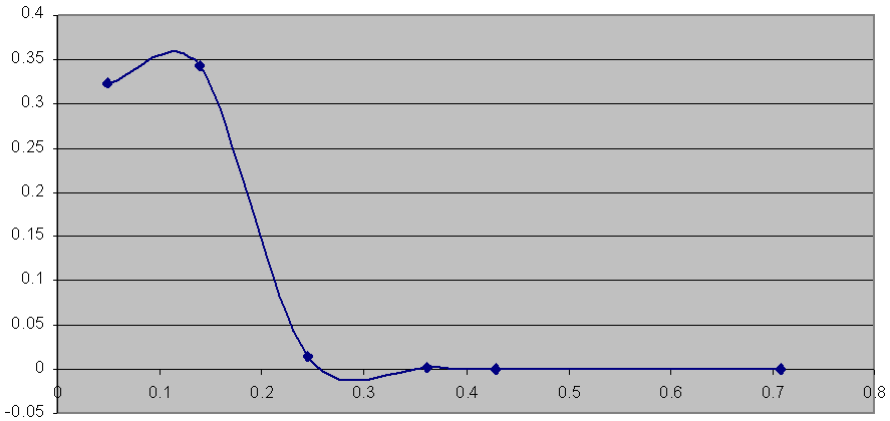

Figure 17. Plot of the function r(α) against α for the shared model system cured at 70°C.

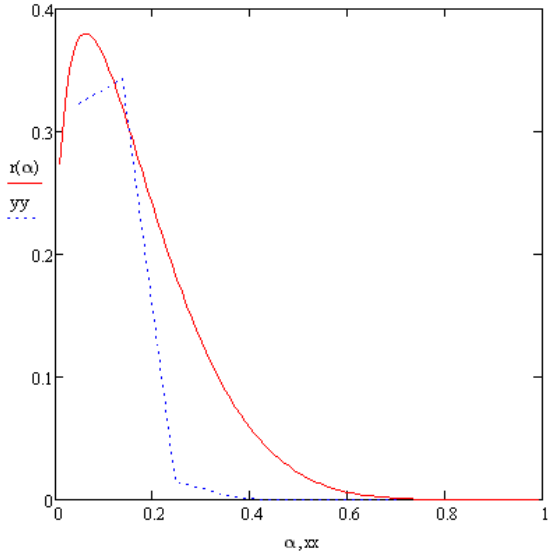

Figure 18. Comparison of theory based on Equation 1 and the experimental function (Figure 17) for the shared model system at 70°C.

The experimental data set for 60°C is shown in Figure 19, and the fitting of the data in Figure 20. The fitting parameters obtained are k_1 = 1.5 x 10^{-2} s^{-1}; k_2 = 16 x 10^{-2} s^{-1}; m = 0.43 and n = 5.

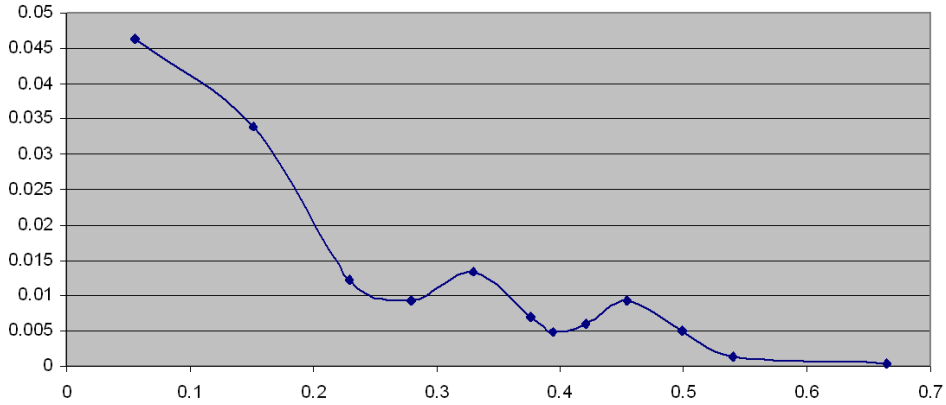

Figure 19. Plot of the function r(α) against α for the shared model system cured at 60°C.

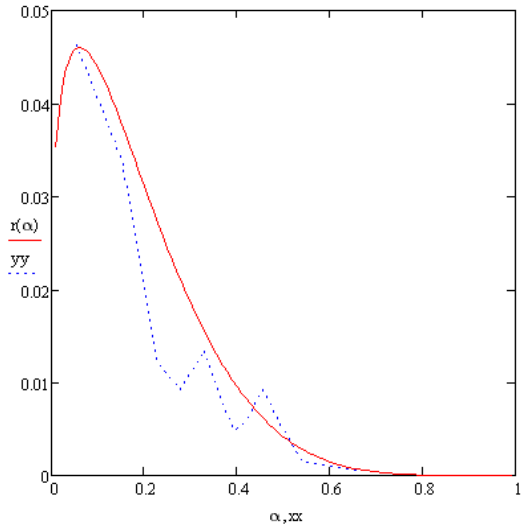

Figure 20. Comparison of theory based on Equation 1 and the experimental function (Figure 19) for the shared model system at 60°C.

The experimental data set for 50°C is shown in Figure 21, and the fitting of the data in Figure 22 . This system shows a very fast cure over the initial 0.2 conversion. The fitting parameters obtained are $k_1 = 0.01 \times 10^{-2}\ s^{-1}$; $k_2 = 10 \times 10^{-2}\ s^{-1}$; m = 0.4 and n = 10. To achieve the peak at low conversion it is necessary to use a high value of n. This is the order of the reaction and such a high value does not really have any molecular significance other than to indicate that the system is highly catalysed.

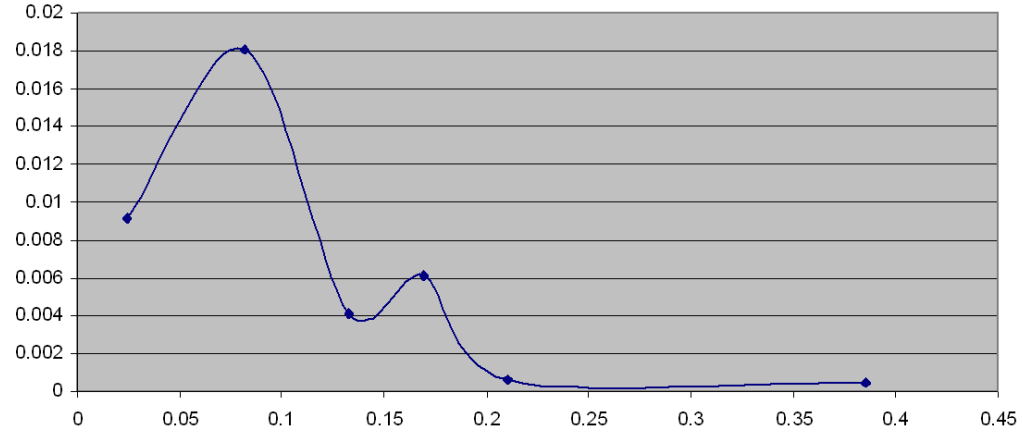

Figure 21. Plot of the function r(α) against α for the shared model system cured at 50°C.

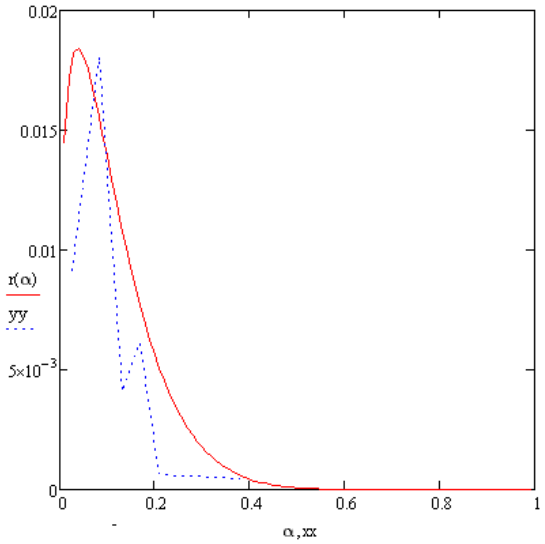

Figure 22. Comparison of theory based on Equation 1 and the experimental function (Figure 21) for the shared model system at 50°C.

Prime20

The data set for Prime20 was similarly fitted to the equation described above and the data at 50°C is shown in Figure 23. The comparison of the theoretical and experimental results is shown in Figure 24, with fitting parameters being k_1 = 2.3 x 10^{-5} s^{-1}; k_2 = 42 x 10^{-5} s^{-1}; m = 0.5 and n= 7. It was found that the fit was very sensitive to the values of m and n.

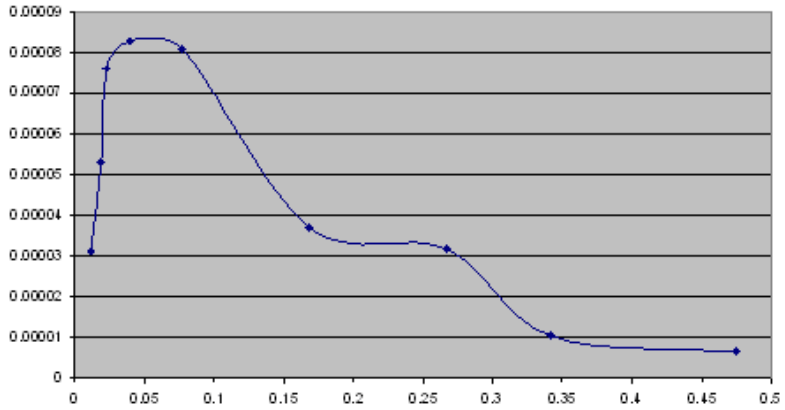

Figure 23. Plot of the function r(α) against α for Prime20 cured at 50°C.

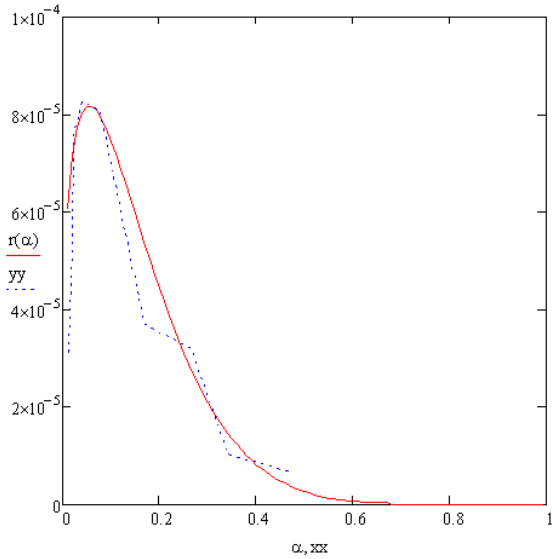

Figure 24. Comparison of theory based on Equation 1 and the experimental function (Figure 23) for Prime20 at 50°C.

Figure 25 and Figure 26 show the plots for Prime20 at 60°C. The values of the fitting coefficients are k_1 = 1 x 10^{-3} s^{-1}; k_2 = 55 x 10^{-3} s^{-1}; m = 0.5 and n = 5. Once more the fitting was very sensitive to the value of n and m. The overall fit of the data is fairly good.

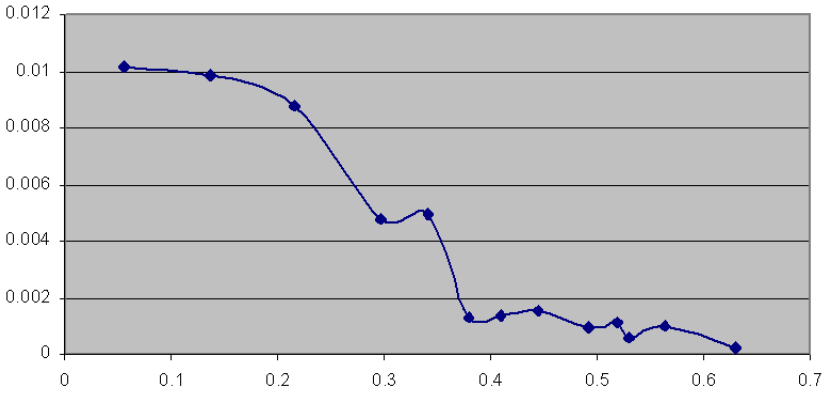

Figure 25. Plot of the function r(α) against α for Prime20 cured at 60°C.

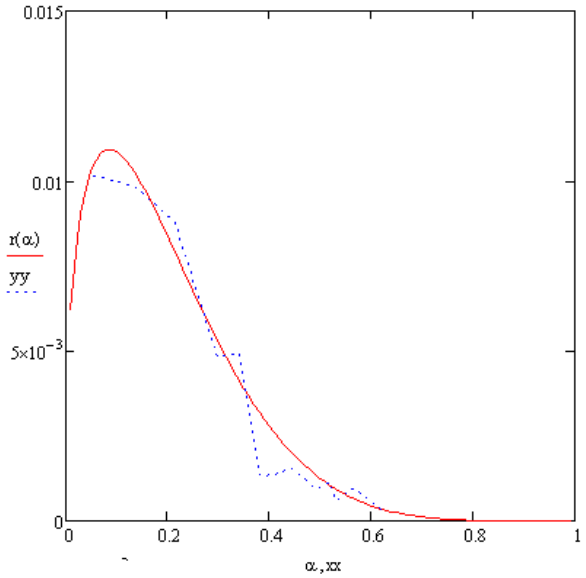

Figure 26. Comparison of theory based on Equation 1 and the experimental function (Figure 25) for Prime20 at 60°C

Figure 27 and Figure 28 show the plots for Prime20 at 70°C. The fitting parameters for PR20 at 70^0C are $k_1 = 1 \times 10^{-2}\ s^{-1}$; $k_2 = 25 \times 10^{-2}\ s^{-1}$; m = 0.5 and n = 6.

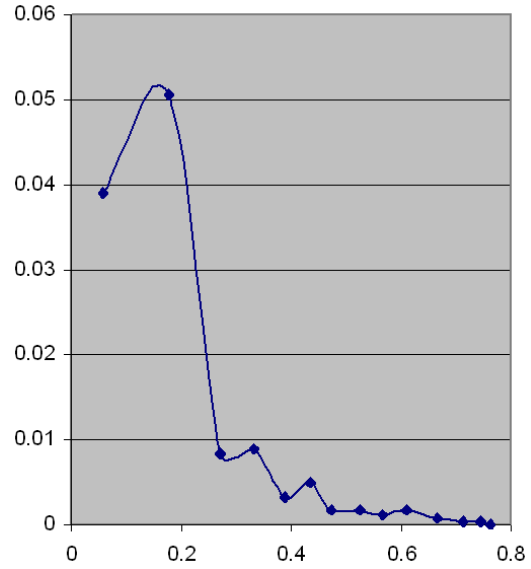

Figure 27. Plot of the function r(α) against α for Prime20 cured at 70°C.

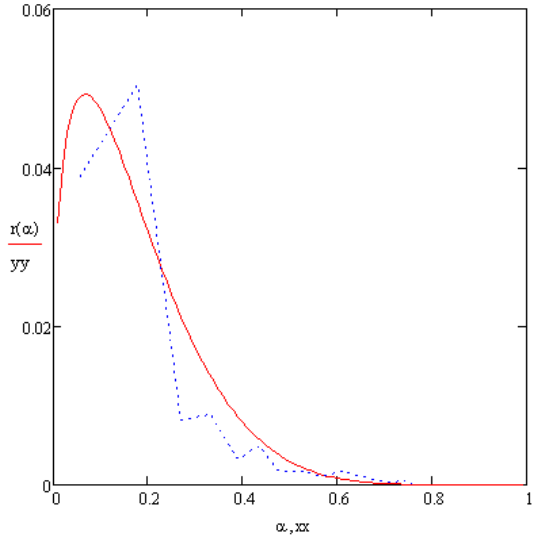

Figure 28. Comparison of theory based on Equation 1 and the experimental function (Figure 27) for Prime20 at 70°C.

SUMMARY OF FITTED DATA.

The parameters obtained form fitting the FTIR data are summarised below, Table 1. Comments can be made about the data as in the section below the table.

Table 1. Summary of the fitting parameters for the molecular systems investigated.

System/Temp	k_1	k_2	m	n
PR55				
35°C	8×10^{-3}	8×10^{-3}	0.5	3.3
30°C	$1.x\ 10^{-3}$	1.3×10^{-2}	0.5	3.0
25°C	1×10^{-3}	2.3×10^{-3}	0.05	2.0
Prime20				
50°C	2.3×10^{-5}	42×10^{-5}	0.5	7
60°C	1×10^{-3}	55×10^{-3}	0.5	5
70°C	1×10^{-2}	25×10^{-2}	0.5	6
Shared Model				
50°C	0.01×10^{-2}	10×10^{-2}	0.4	10
60°C	1.5×10^{-2}	16×10^{-2}	0.43	5
70°C	$11x\ 10^{-2}$	180×10^{-2}	0.5	6
Strathclyde model				
30°C	1×10^{-4}	15×10^{-2}	0.5	0.48
30°C repeat	0.1×10^{-4}	17×10^{-2}	0.5	0.5
35°C	0.01×10^{-2}	21×10^{-2}	0.8	1
35°C repeat	0.1×10^{-2}	41×10^{-2}	1.5	0.4
40°C	0.1×10^{-2}	41×10^{-2}	1.5	0.4
40°C repeat	0.05×10^{-2}	41×10^{-2}	1.5	0.5
45°C	0.05×10^{-2}	62×10^{-2}	1.5	0.5
45°C repeat	0.5×10^{-2}	51×10^{-2}	1.6	0.7
50°C	1×10^{-2}	51×10^{-2}	1.6	0.4

Strathclyde Model System

This is the system which was most extensively investigated. At 30°C the fitting parameters with m = 0.5 and n 0.5 are close to what would be expected for an epoxy system. The fit is not particularly good at low values of α which raises questions about the fit in relation to m and n.

Raising the temperature to 35°C gives a better fit of the data however there is still an uncertainty as indicated by the differences in the fitting parameters between the two sets of data. The first fit neglects the last data point and is probably better than the fit of the repeat data.

Raising the temperature to 40°C gives a good level of repeatability in the data and the fitting parameters indicating that the data has a higher level of reliability.

Raising the temperature to 45°C leads to fits which are very different between the original and repeat data. The values of k obtained are very different for the original and repeat data - reflecting the high level of scatter in the original $r(\alpha)$ function. The scatter leads to a high degree of uncertainty in the value of k_1, however the mean value of k_2 shows the expected increase with increase in temperature.

The function $r(\alpha)$ at 50°C shows a very high degree of scatter which makes the fitting very questionable. The values obtained do not show the progression which would be expected from extrapolation of the lower temperature values.

Shared Model System

The values of k increase with increasing temperature. The values of m are essentially independent of temperature whereas the values of n decrease with temperature. The fits are however not very convincing and raise questions about the reliability of the analysis.

PR55

The value of k_1 increase with increasing temperature however the values of k_2 do not. The value of m appears to change very little with temperature whereas the value of n increases with increasing temperature. The fit at 25°C is not very convincing at high values of α and it may therefore be assumed that the values of k at 25°C must be considered to be a little suspect.

Prime 20

The values of k_1 and k_2 show a smooth progression with increasing temperature and the values of m and n are approximately independent of temperature which suggests that the fits are good and that the data is reliable.

REFERENCES

1. Kamal Kamal, M.R., *Thermoset Characterisation for Moldability Analysis.* Polymer Engineering Science, 1974. **14:** p. 231-239.

APPENDIX B: DIELECTRIC DATA

The data below is supplementary to that presented within *Chapter 7. Results (IV): Cure Characterisation: Dielectrics*.

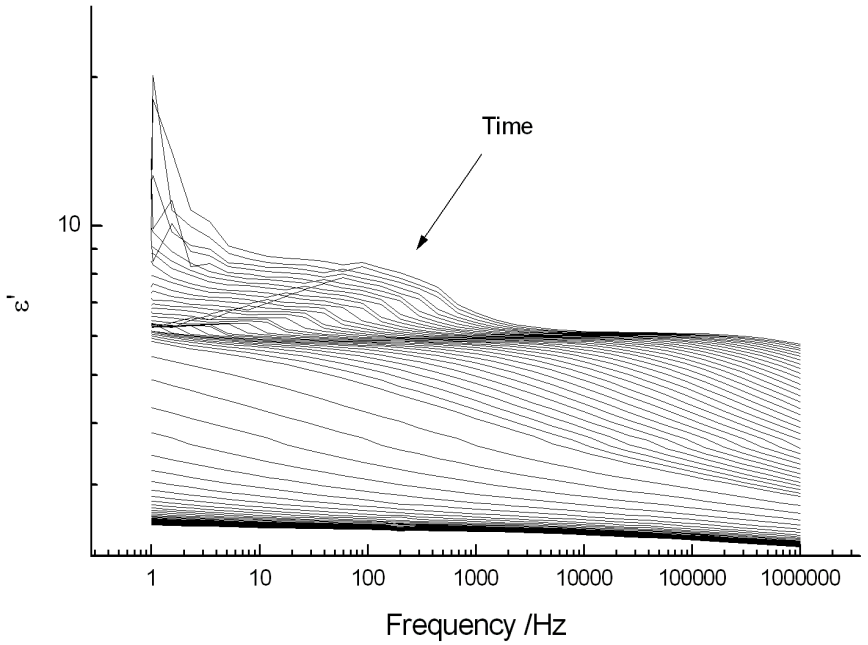

Figure 29. Plot of real permittivity for the Strathclyde model system cured at room temperature as a function of cure time.

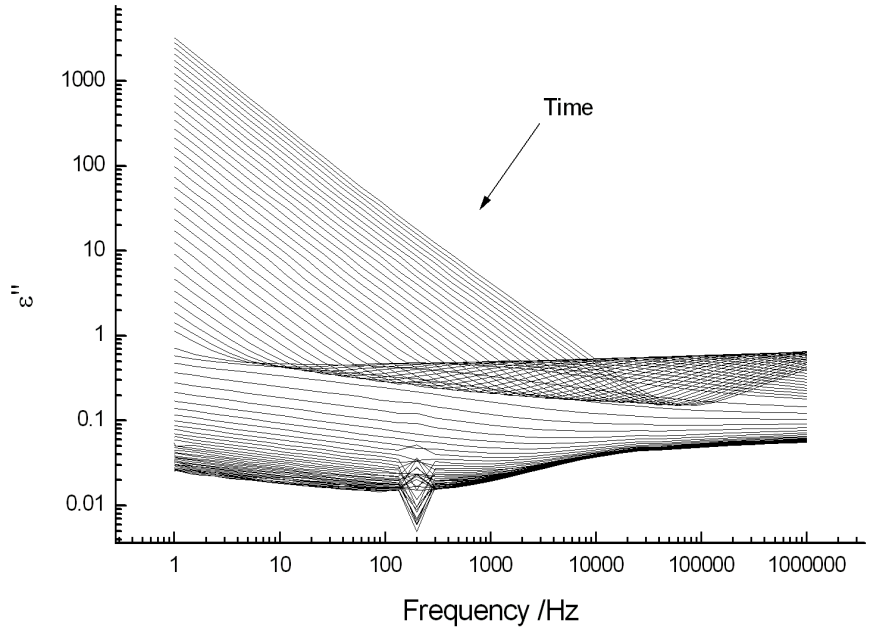

Figure 30. Plot of imaginary permittivity for the Strathclyde model system cured at room temperature as a function of cure time.

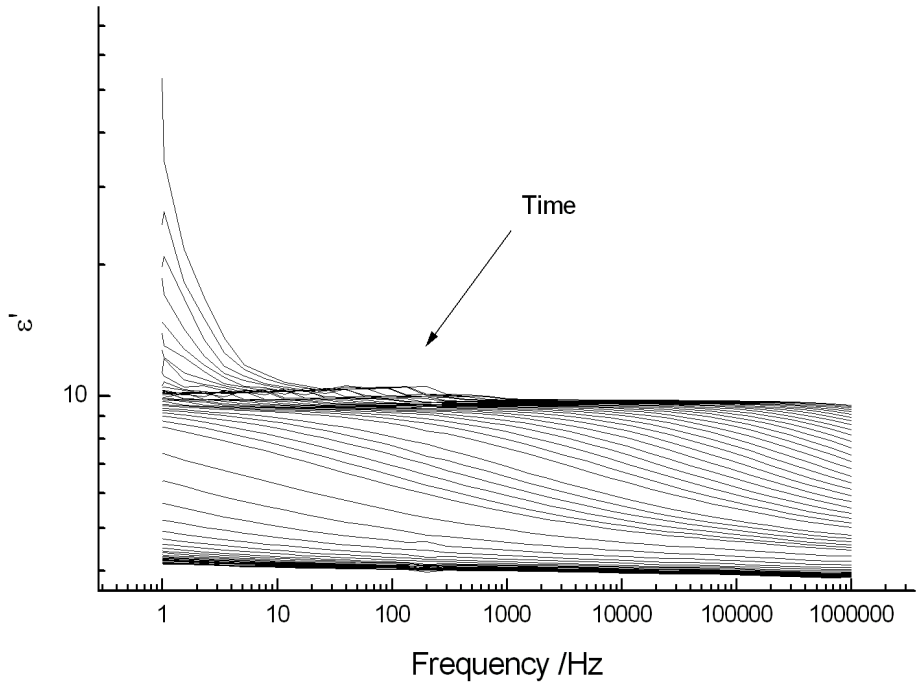

Figure 31. Plot of real permittivity for the Strathclyde model system cured at 30°C as a function of cure time.

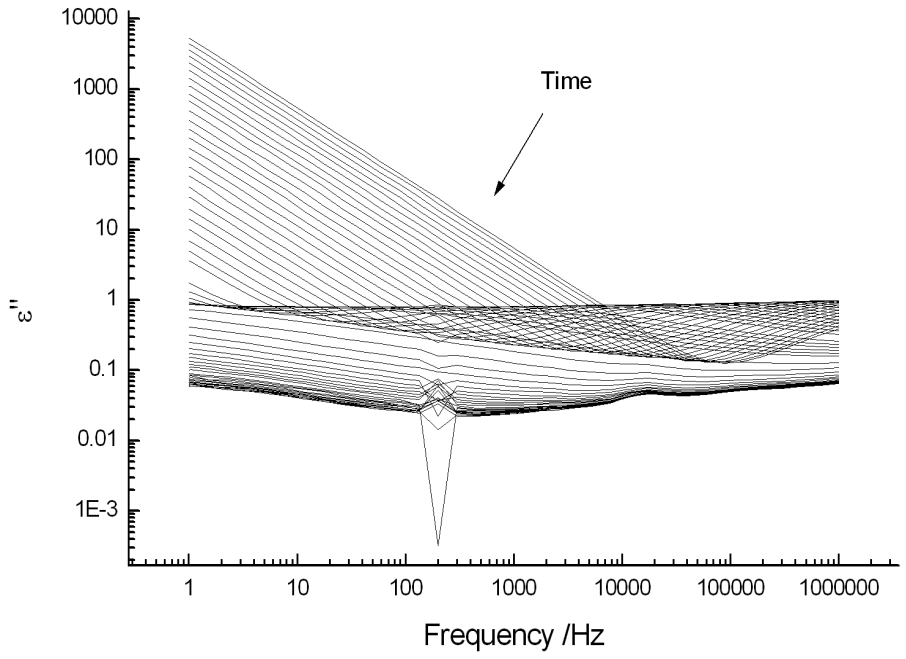

Figure 32. Plot of imaginary permittivity for the Strathclyde model system cured at 30°C as a function of cure time.

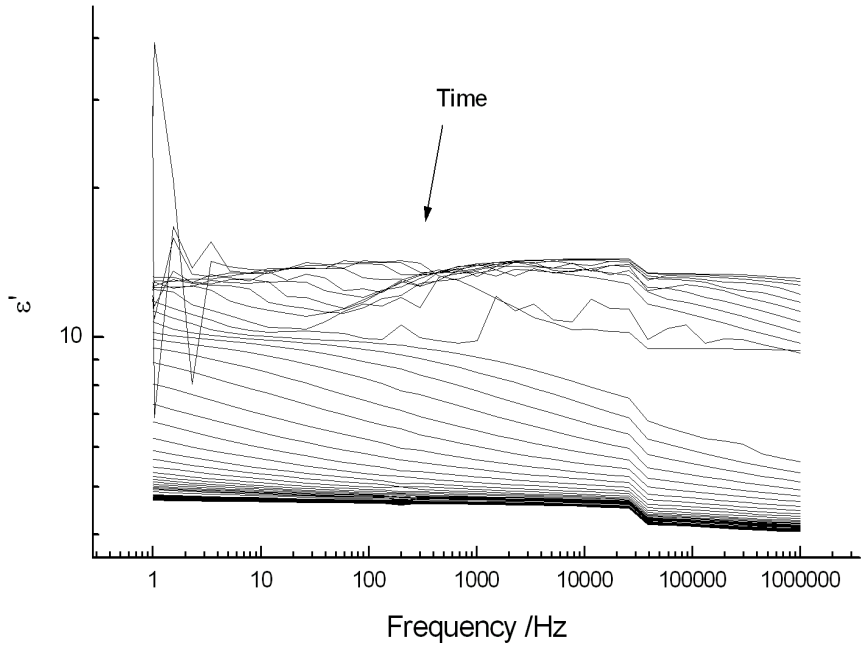

Figure 33. Plot of real permittivity for the Strathclyde model system cured at 40°C as a function of cure time.

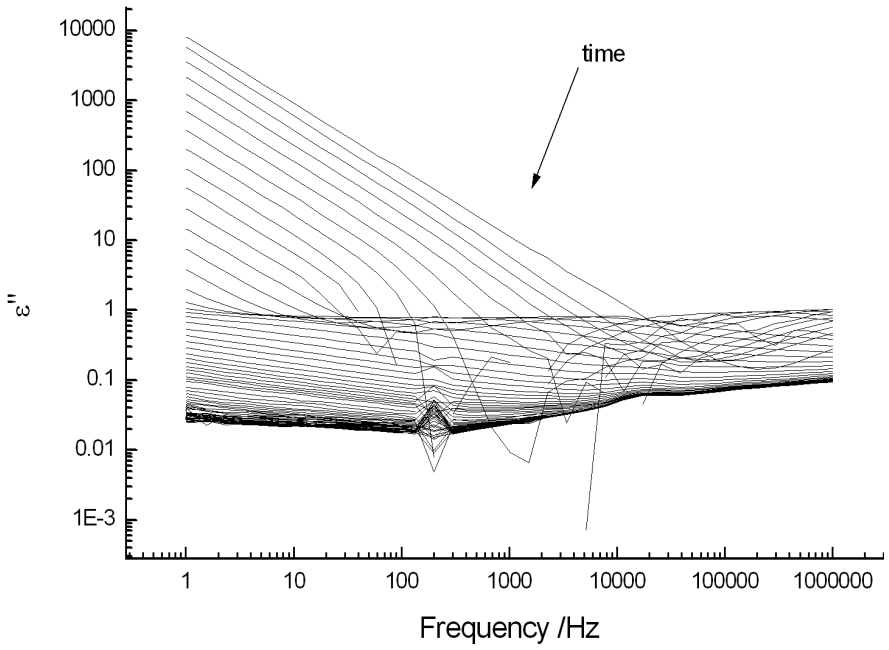

Figure 34. Plot of imaginary permittivity for the Strathclyde model system cured at 40°C as a function of cure time.

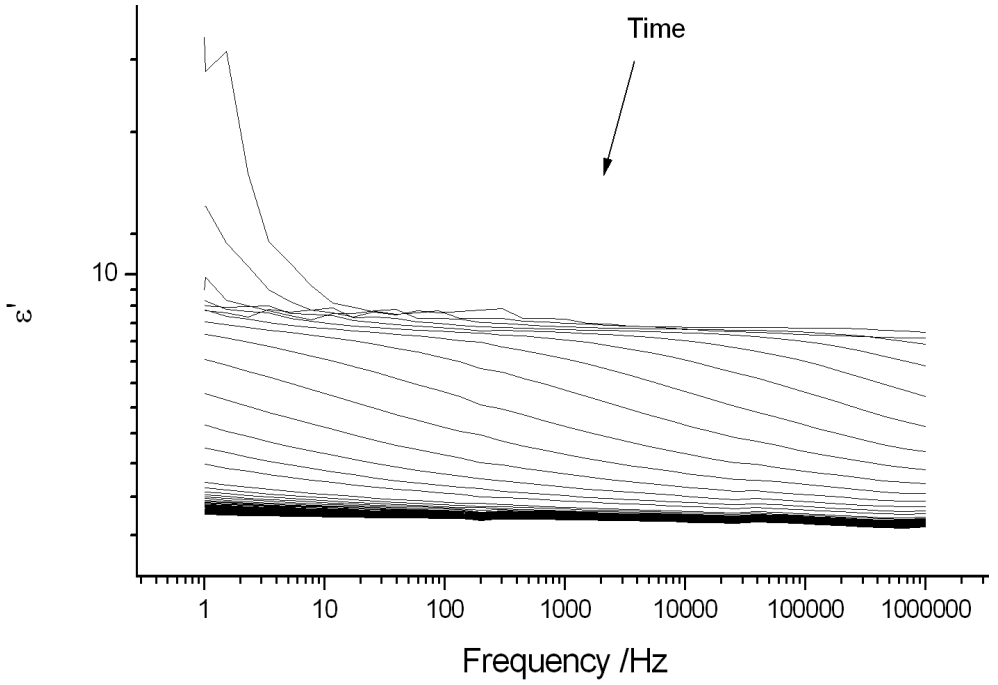

Figure 35. Plot of real permittivity for the Strathclyde model system cured at 50°C as a function of cure time.

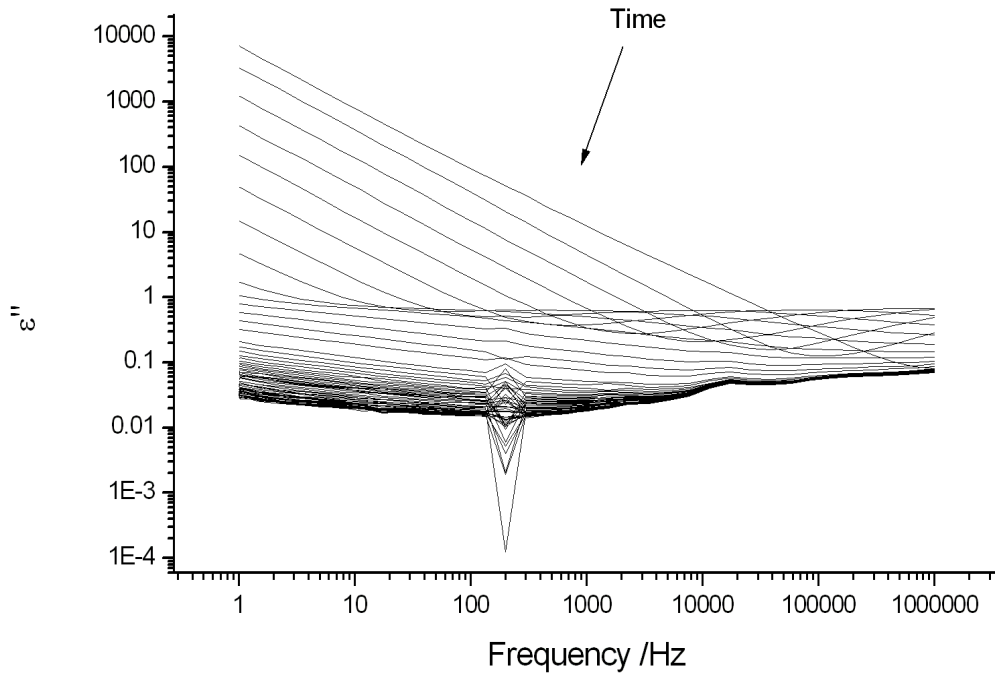

Figure 36. Plot of imaginary permittivity for the Strathclyde model system cured at 50°C as a function of cure time.

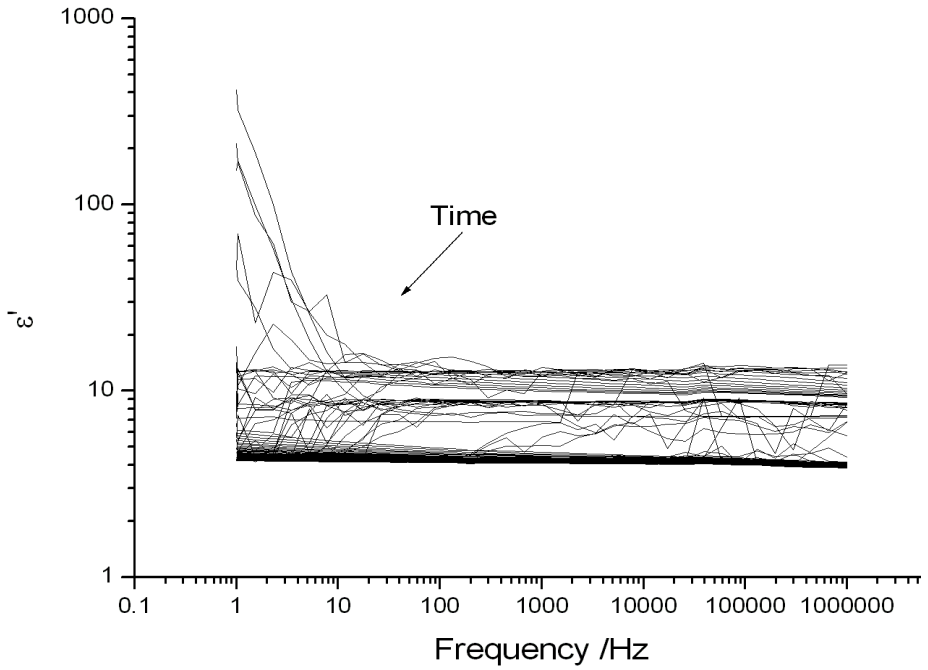

Figure 37. Plot of real permittivity for the shared model system cured at 50°C as a function of cure time.

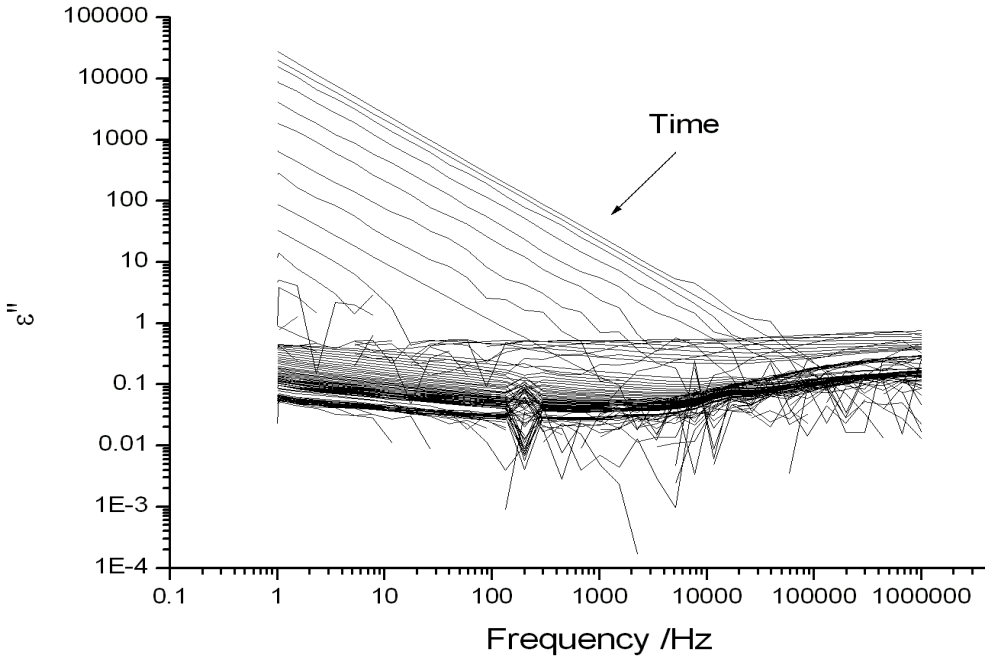

Figure 38. Plot of imaginary permittivity for the shared model system cured at 50°C as a function of cure time.

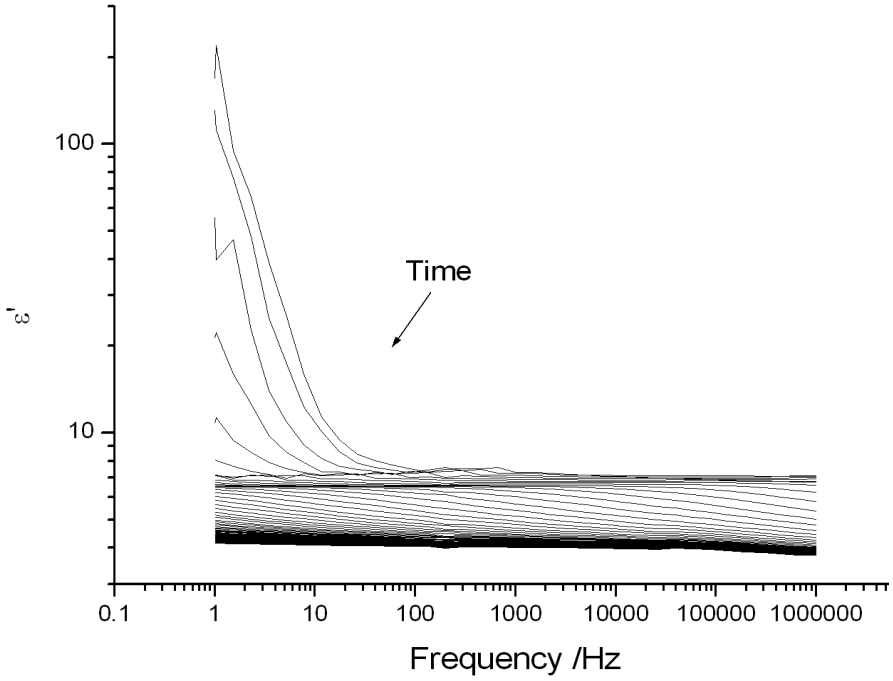

Figure 39. Plot of real permittivity for the shared model system cured at 55°C as a function of cure time.

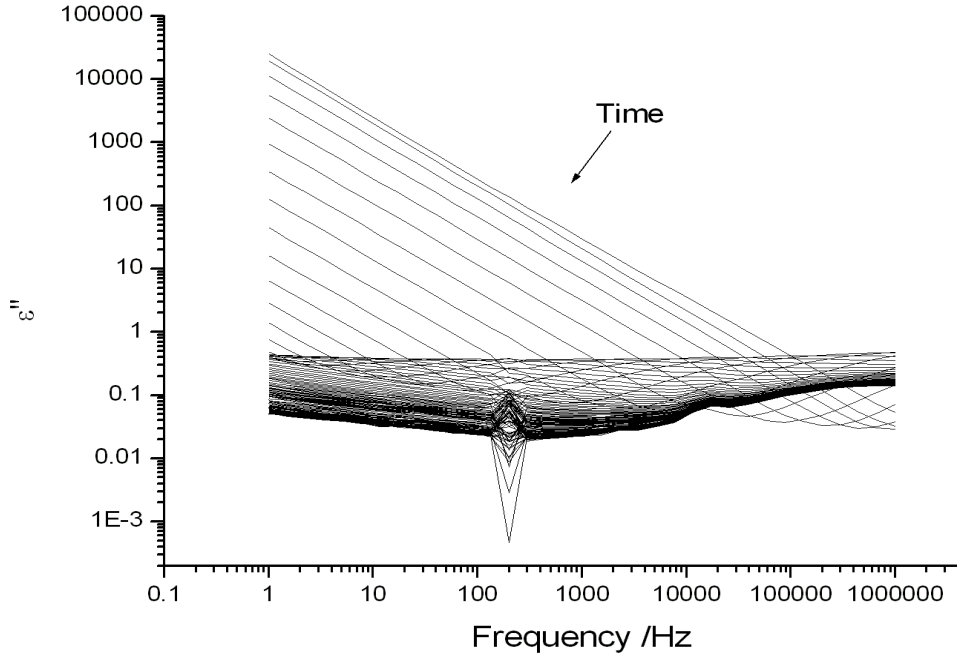

Figure 40. Plot of imaginary permittivity for the shared model system cured at 55°C as a function of cure time.

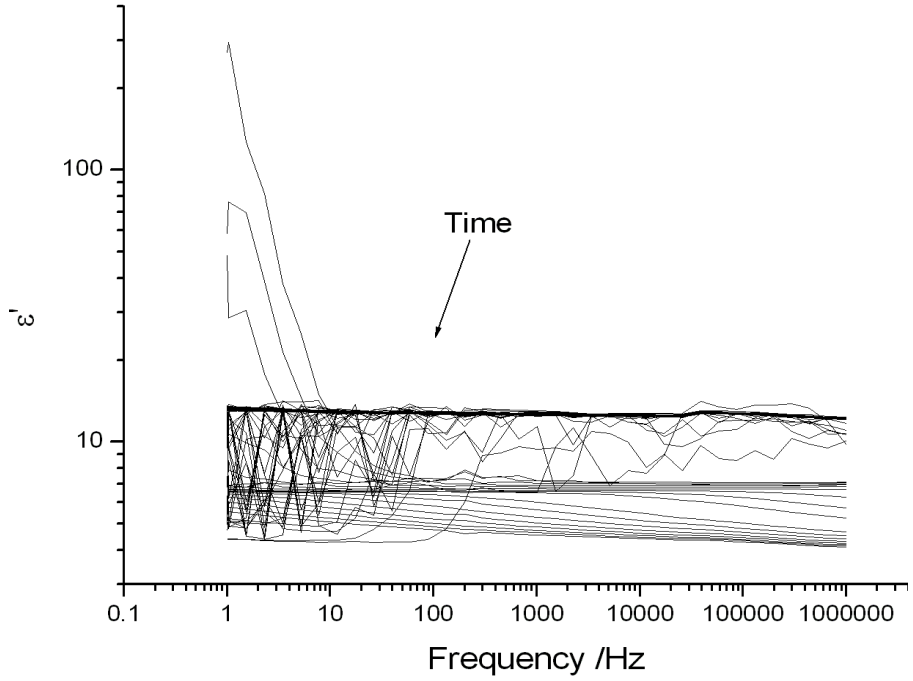

Figure 41. Plot of real permittivity for the shared model system cured at 60°C as a function of cure time.

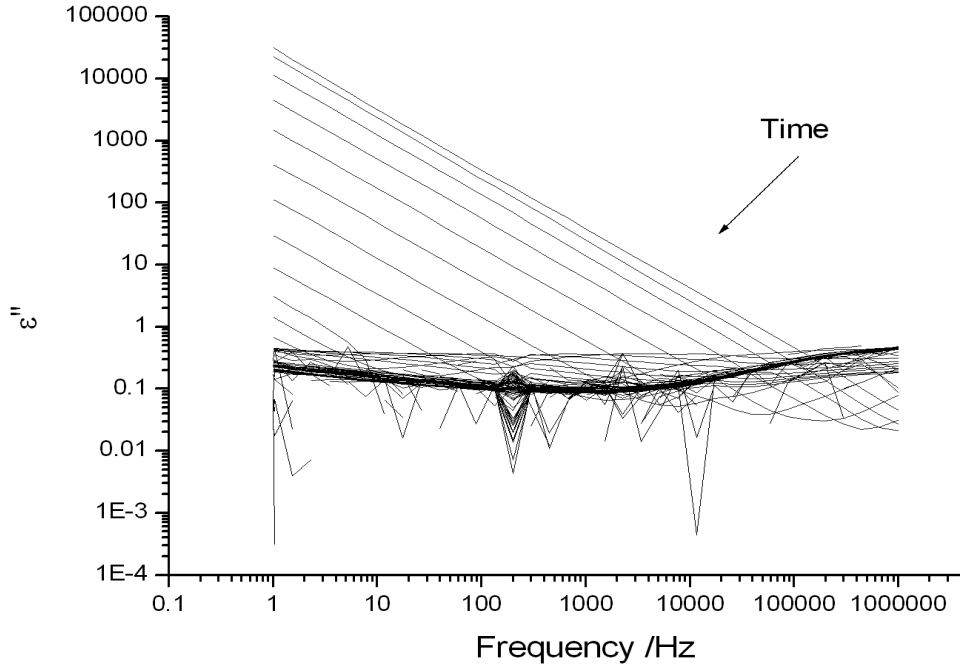

Figure 42. Plot of imaginary permittivity for the shared model system cured at 60°C as a function of cure time.

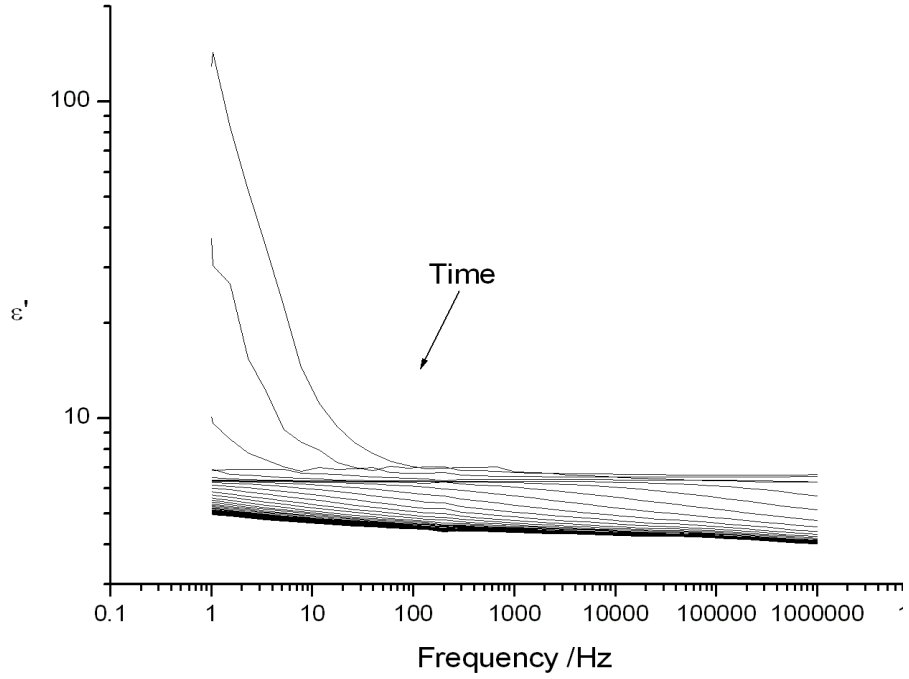

Figure 43. Plot of real permittivity for the shared model system cured at 65°C as a function of cure time.

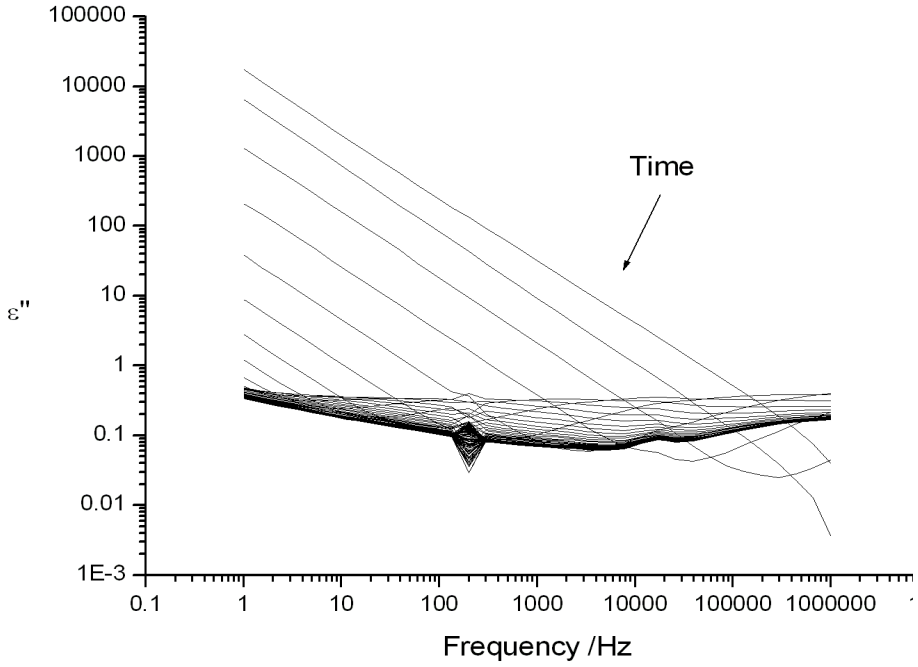

Figure 44. Plot of imaginary permittivity for the shared model system cured at 65°C as a function of cure time.

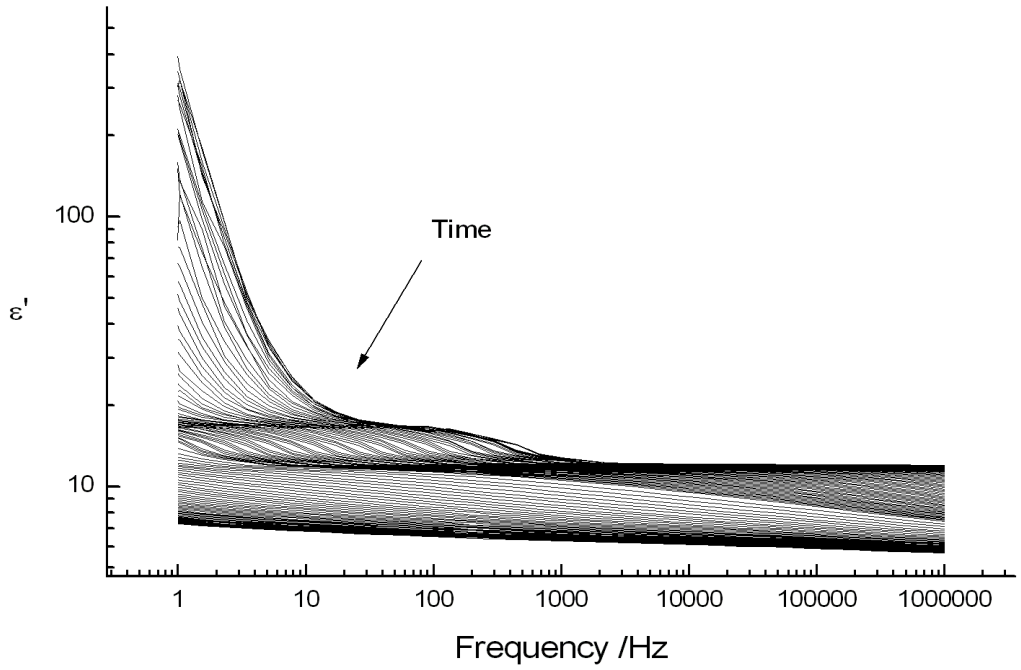

Figure 45. Plot of real permittivity for PR55 cured at 30°C as a function of cure time.

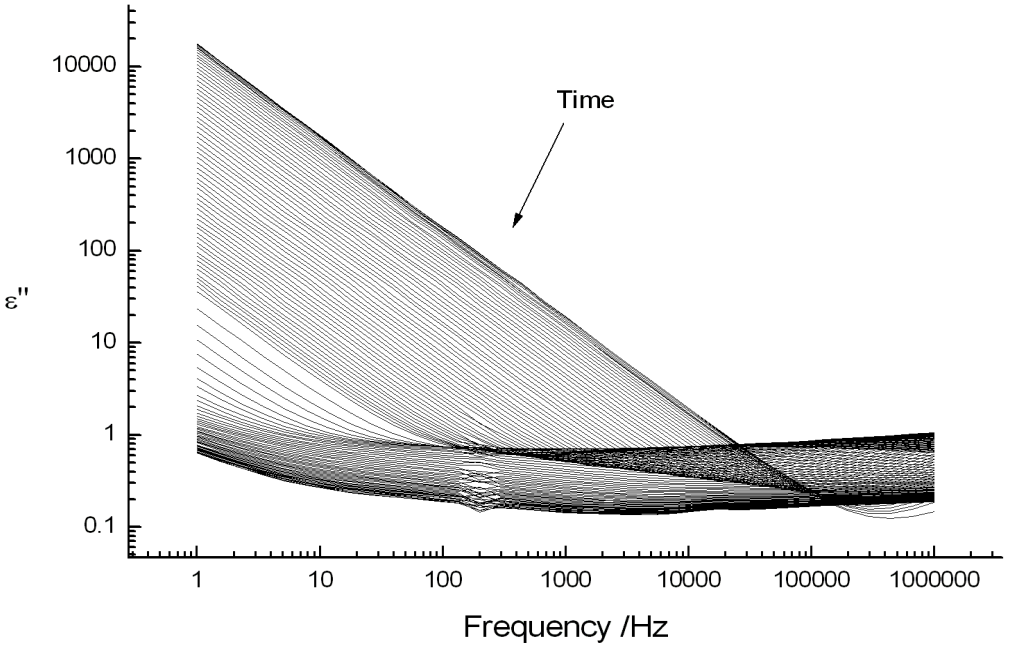

Figure 46. Plot of imaginary permittivity for PR55 cured at 30°C as a function of cure time.

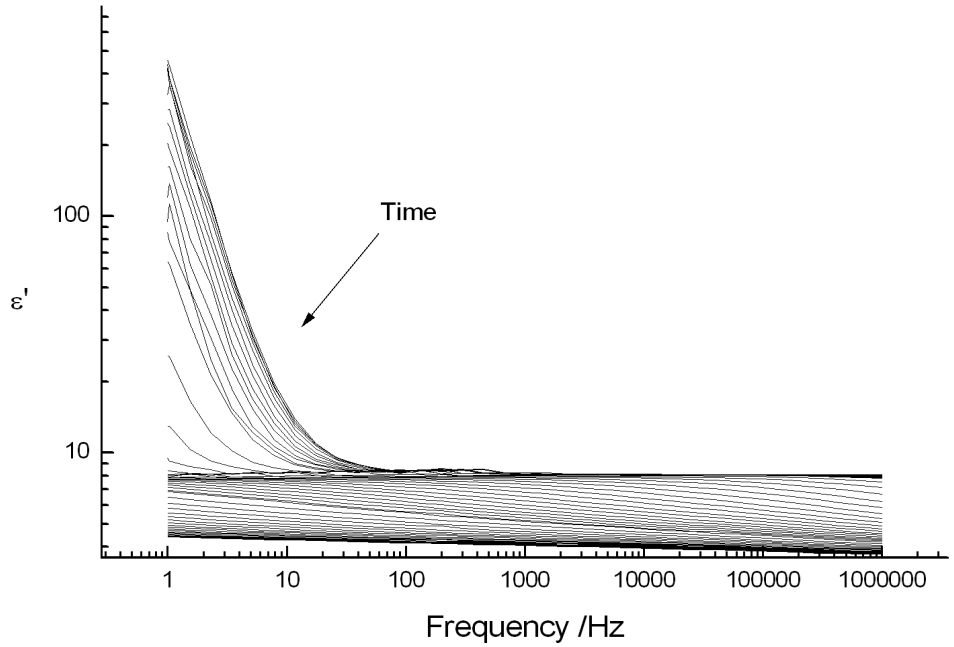

Figure 47. Plot of real permittivity for PR55 cured at 35°C as a function of cure time.

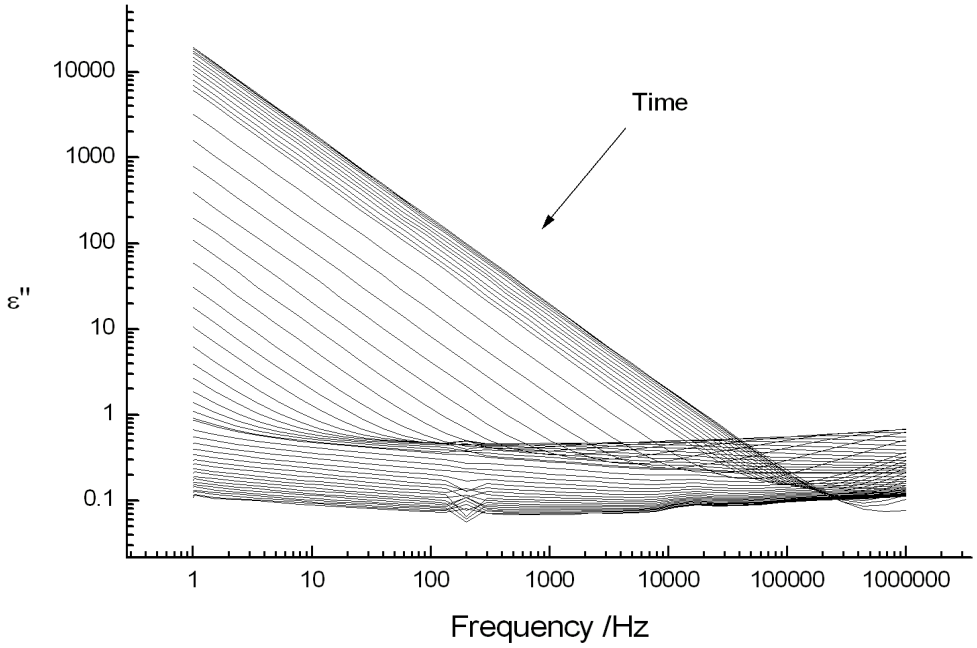

Figure 48. Plot of imaginary permittivity for PR55 cured at 35°C as a function of cure time.

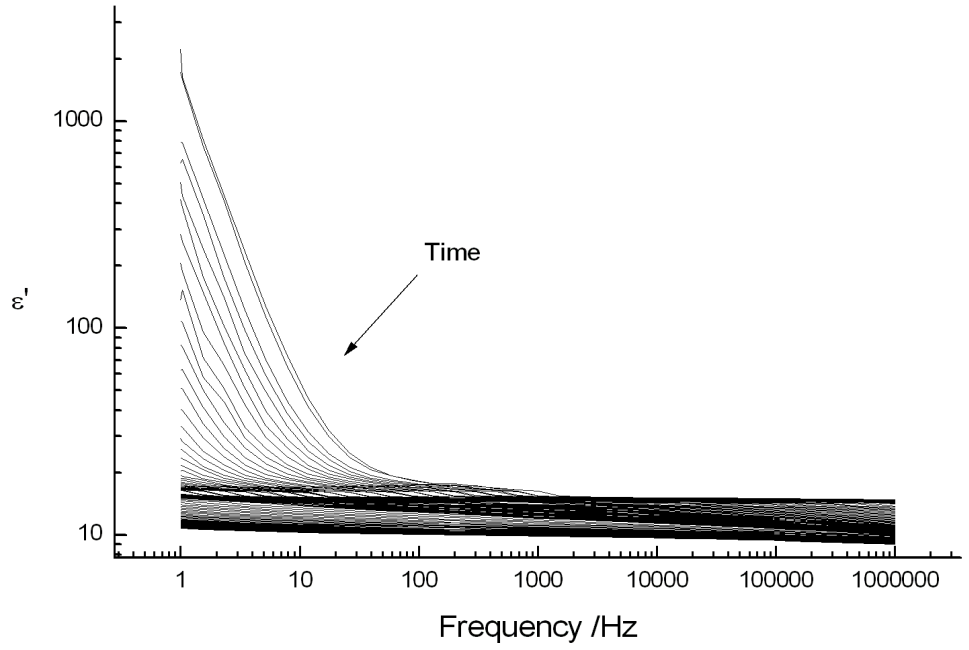

Figure 49. Plot of real permittivity for PR55 cured at 40°C as a function of cure time.

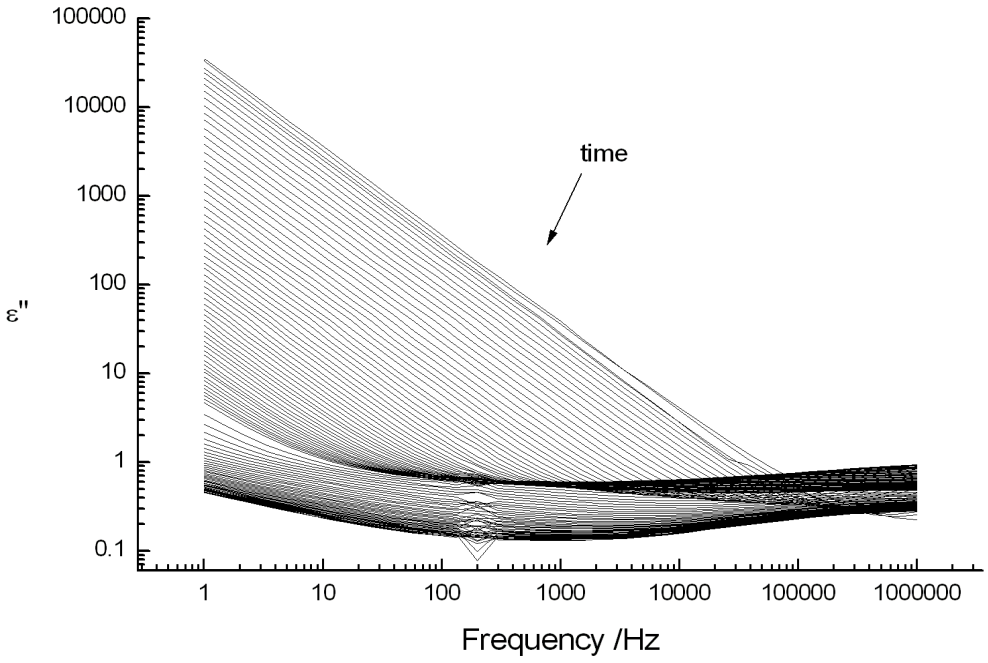

Figure 50 Plot of imaginary permittivity for PR55 cured at 40°C as a function of cure time.

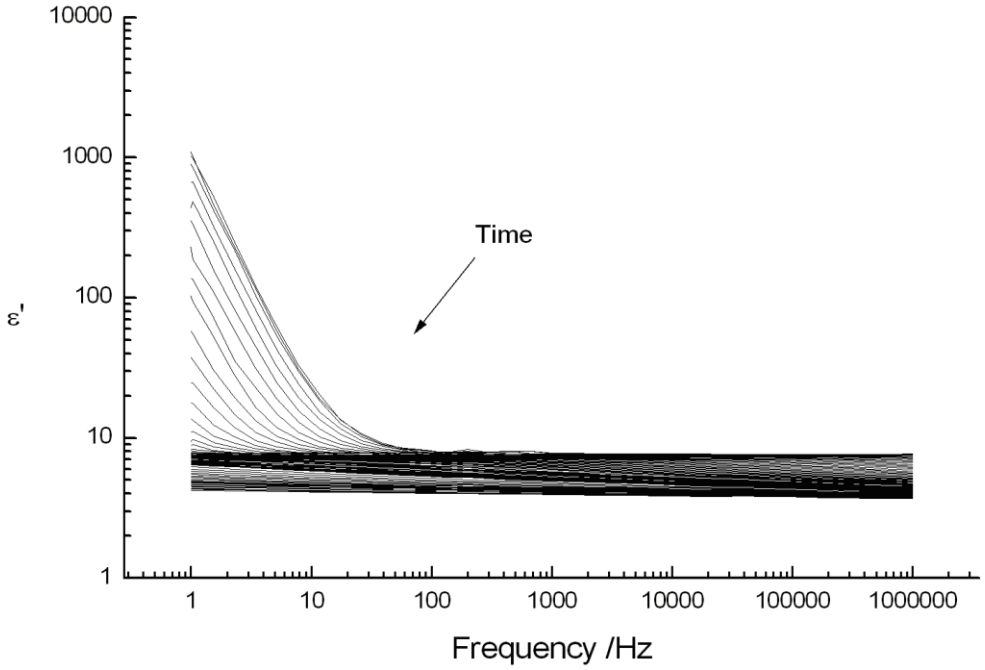

Figure 51. Plot of real permittivity for PR55 cured at 45°C as a function of cure time.

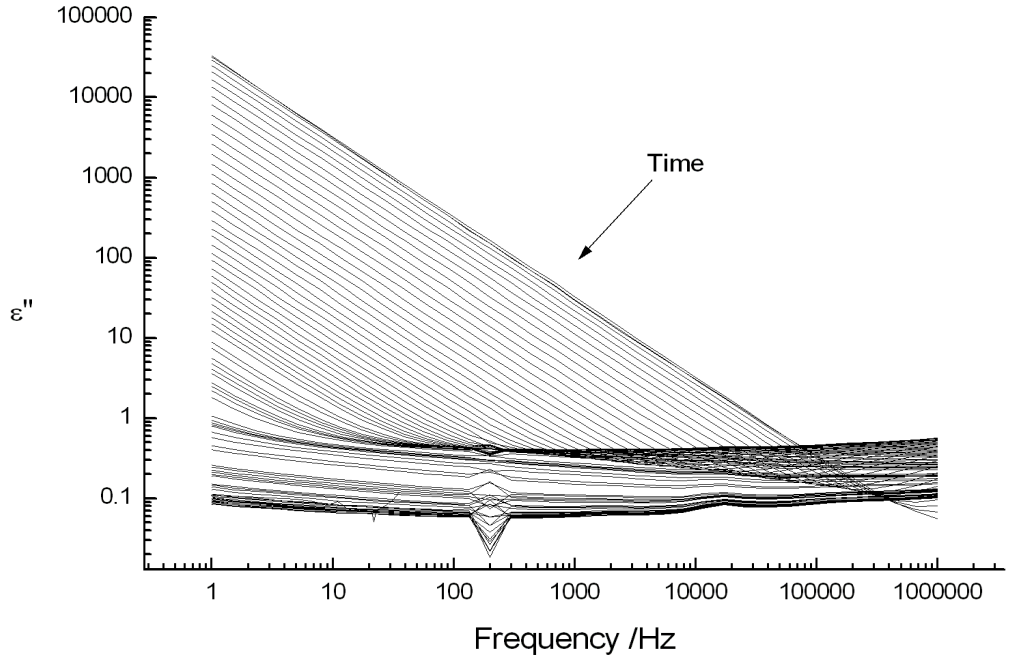

Figure 52. Plot of imaginary permittivity for PR55 cured at 45°C as a function of cure time.

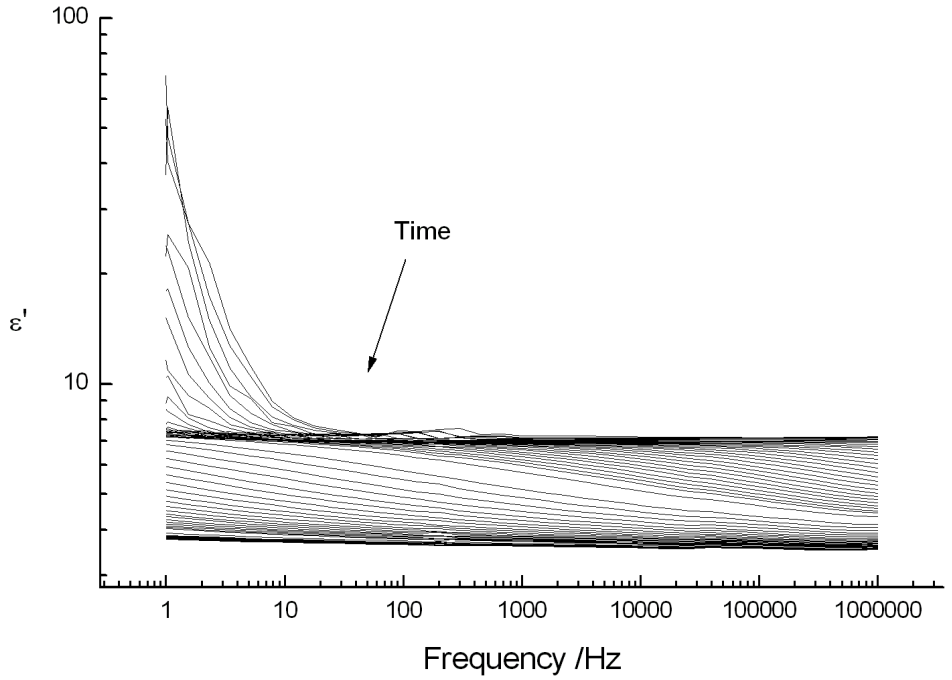

Figure 53. Plot of real permittivity for Prime20 cured at 50°C as a function of cure time.

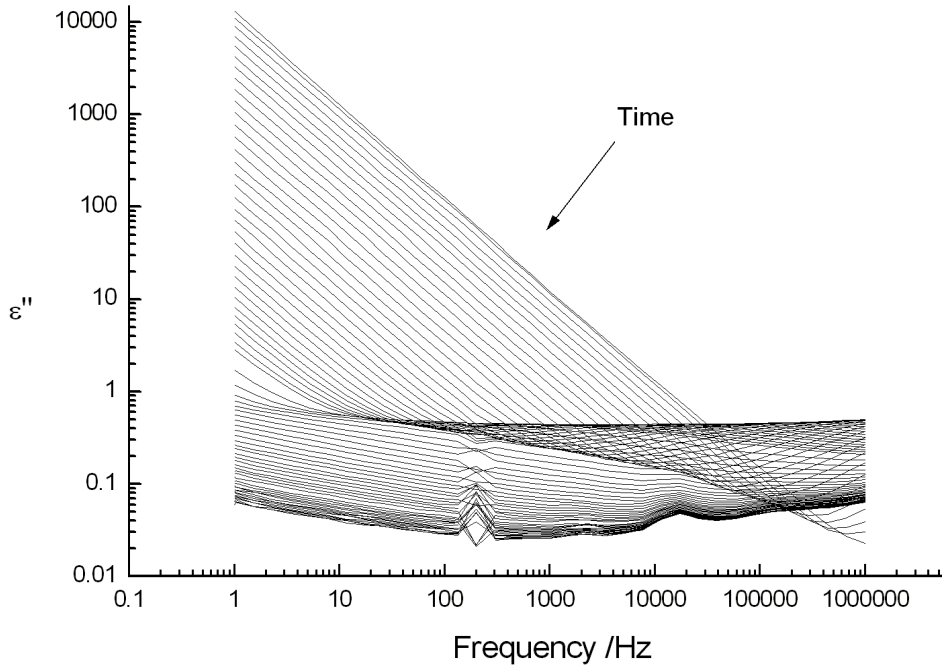

Figure 54. Plot of imaginary permittivity for Prime20 cured at 50°C as a function of cure time.

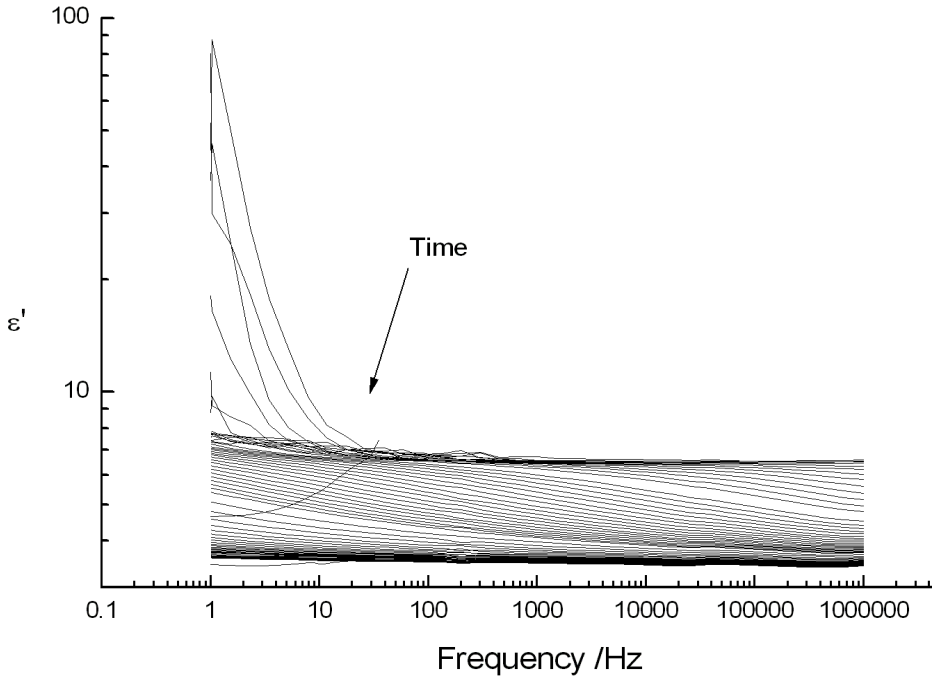

Figure 55. Plot of real permittivity for Prime20 cured at 60°C as a function of cure time.

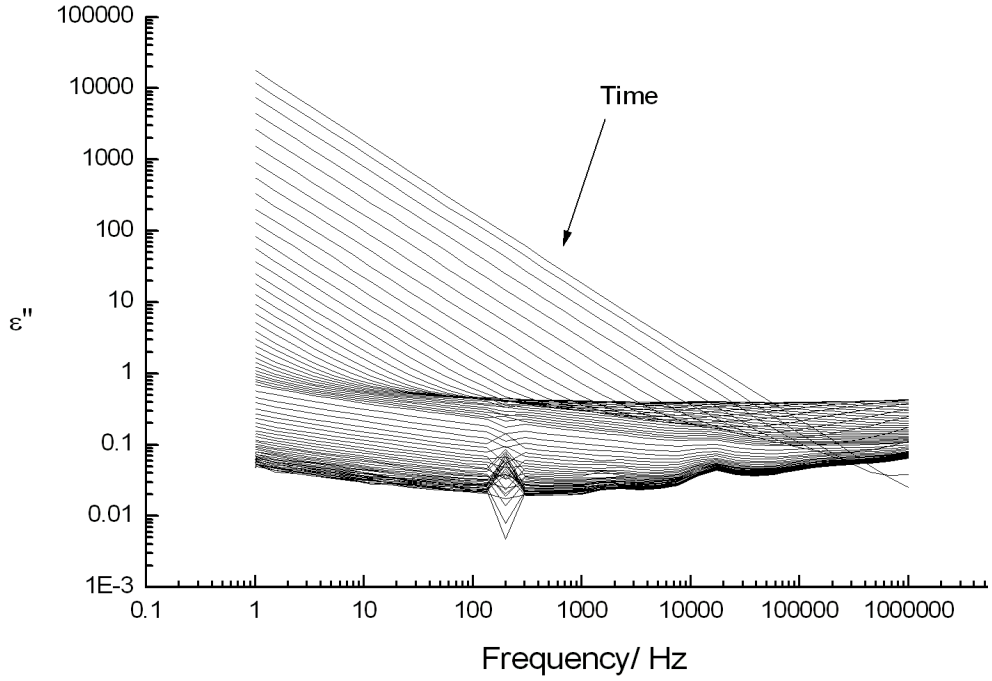

Figure 56. Plot of imaginary permittivity for Prime20 cured at 60°C as a function of cure time.

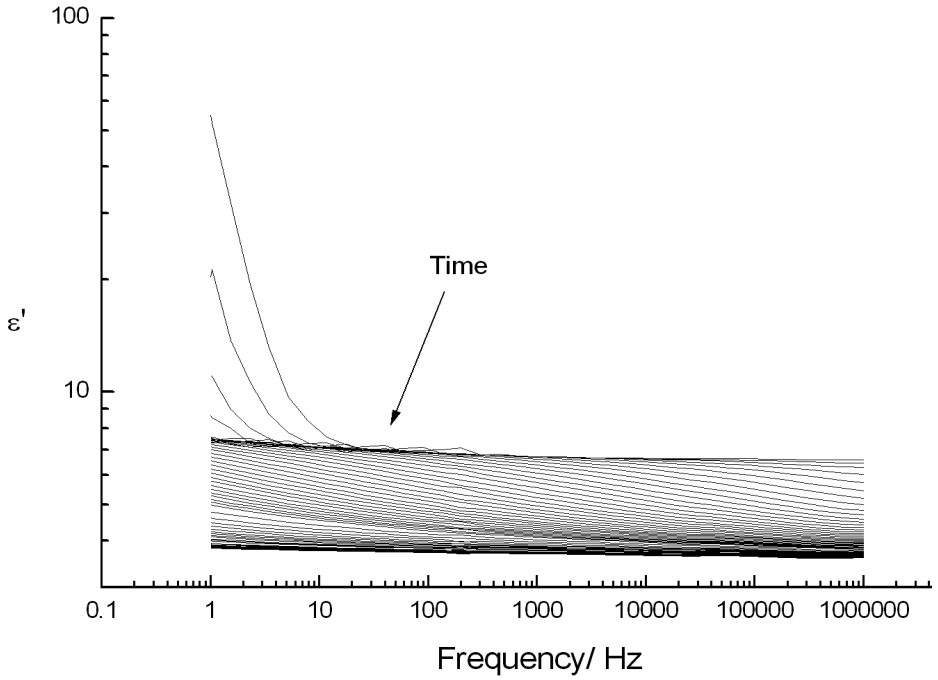

Figure 57. Plot of real permittivity for Prime20 cured at 70°C as a function of cure time.

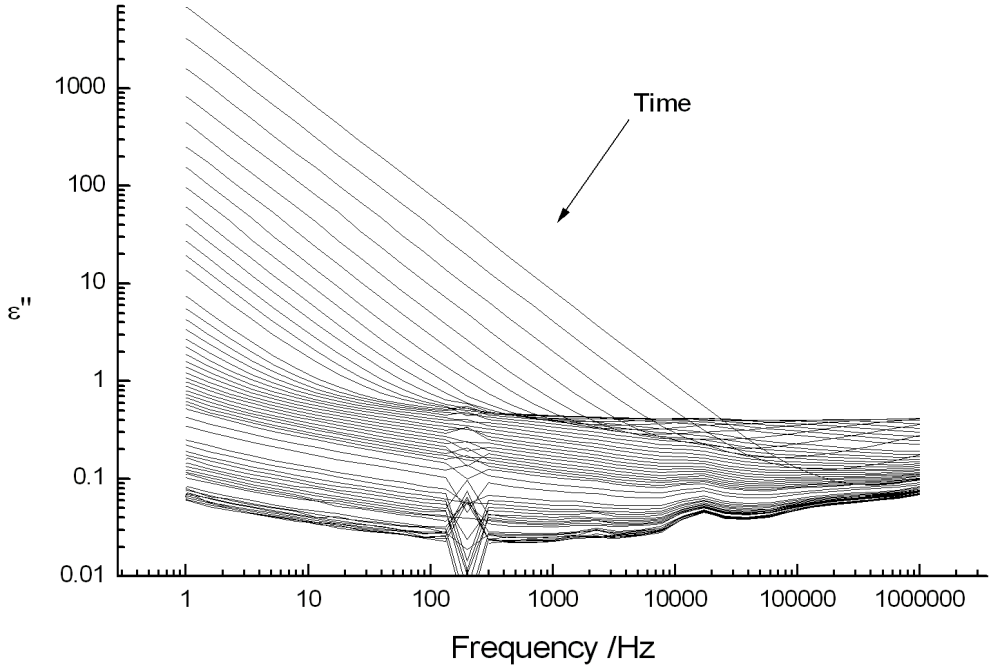

Figure 58. Plot of imaginary permittivity for Prime20 cured at 70°C as a function of cure time.

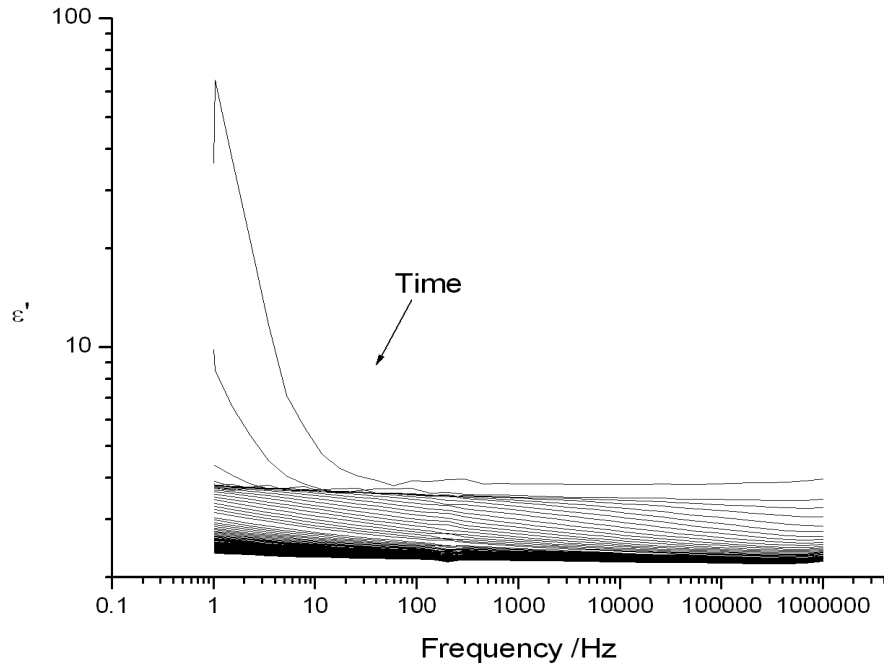

Figure 59. Plot of real permittivity for Prime20 cured at 80°C as a function of cure time.

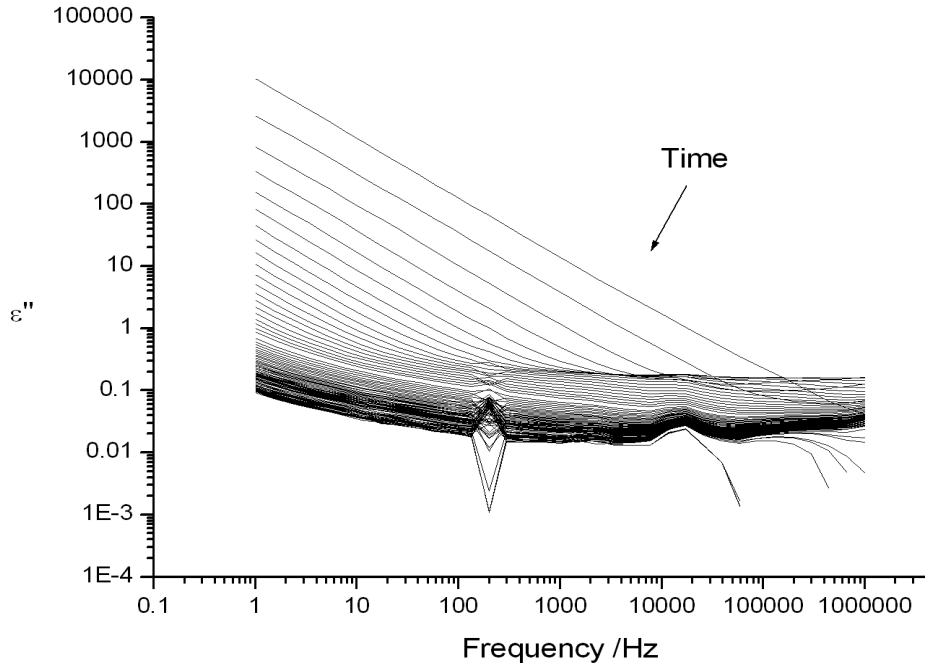

Figure 60. Plot of imaginary permittivity for Prime20 cured at 80°C as a function of cure time.

APPENDIX C: WATER INGRESS SUPPLEMENTARY PLOTS

The plots below are supplementary to that presented within *Chapter 9. Results (VI): Water Ingress*, with the first set being DSC traces.

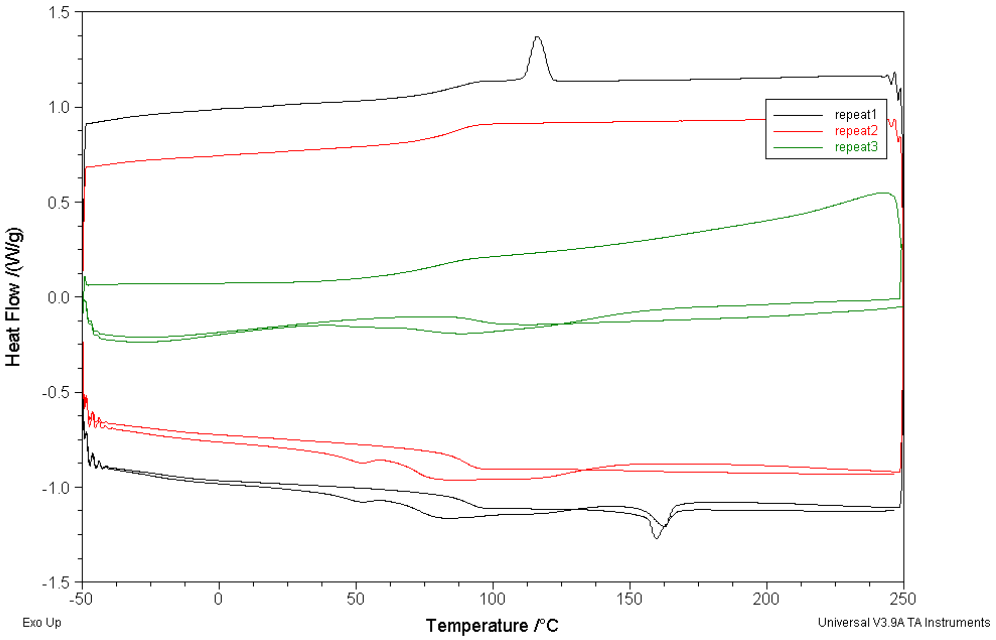

Figure 61. DSC scans of Prime20 system cured at 60ºC.

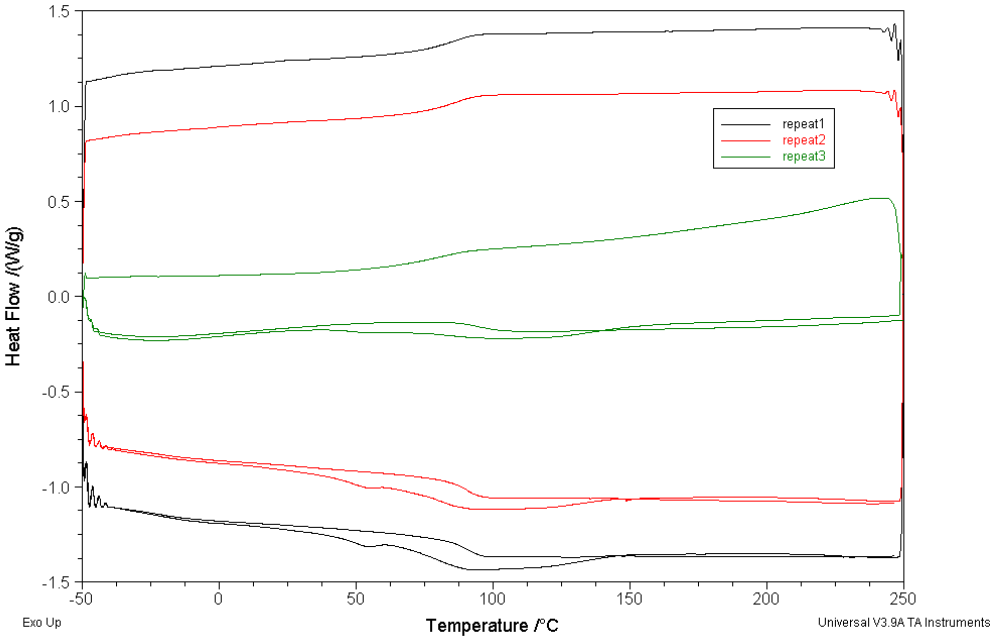

Figure 62. DSC scans of Prime20 system cured at 70ºC.

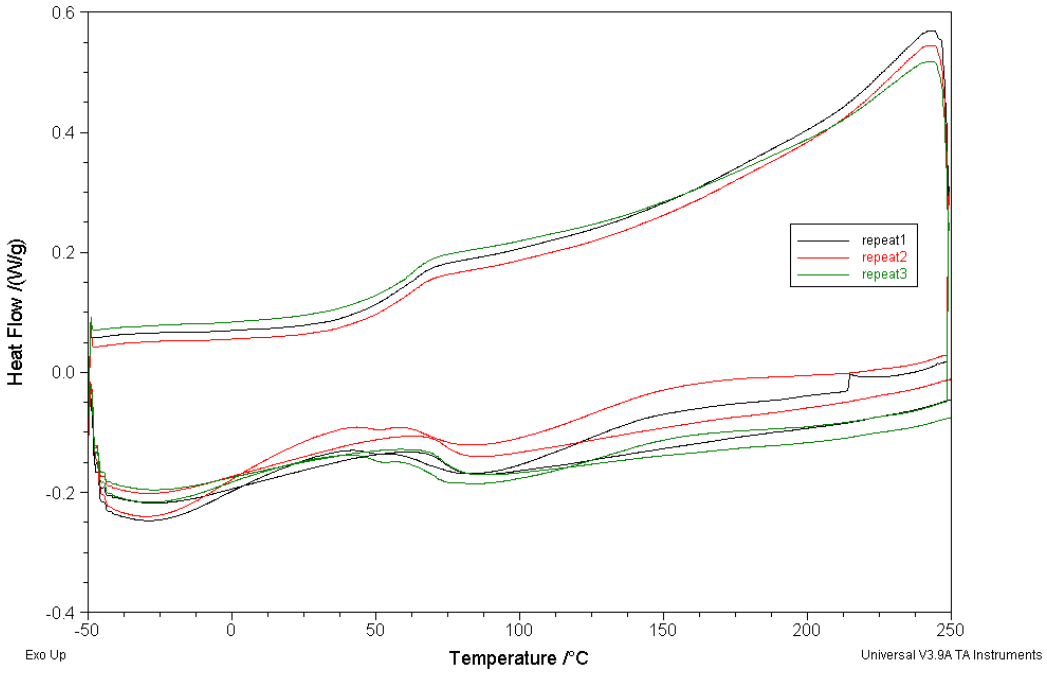

Figure 63. DSC scans of shared model system cured at 60ºC.

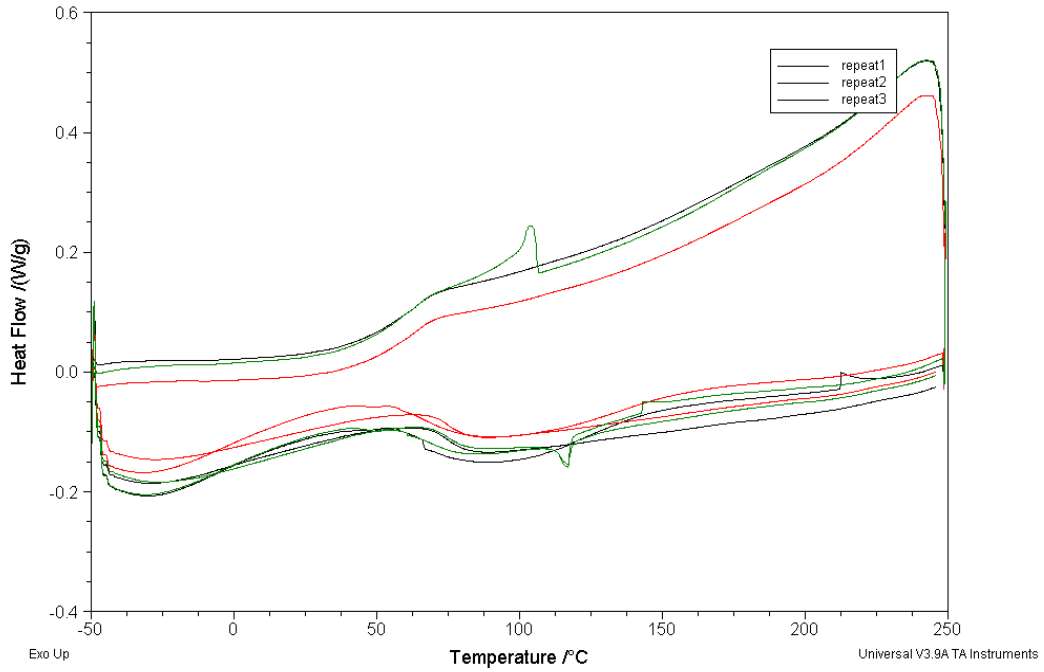

Figure 64. DSC scans of shared model system cured at 70ºC.

Water Ingress HF Dielectric Plots

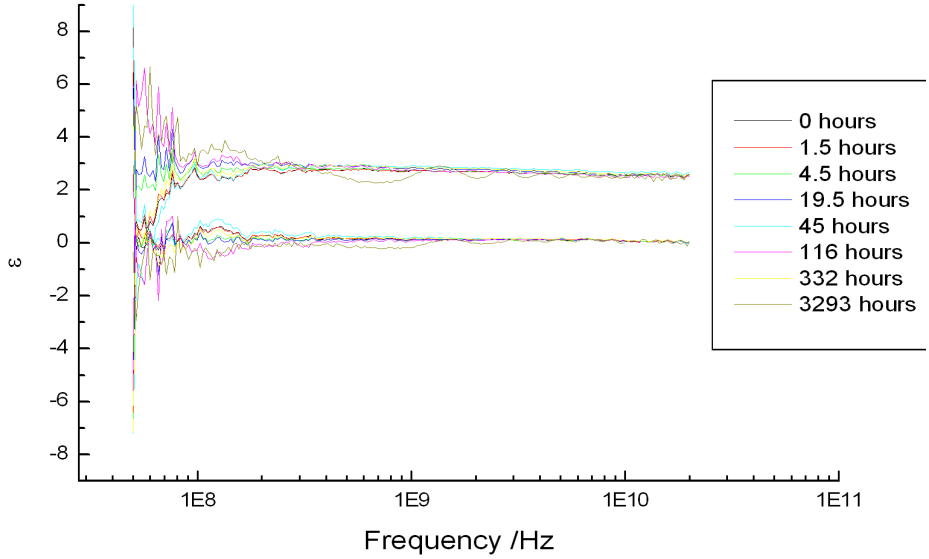

Figure 65. Changes in real permittivity (top set of lines) and imaginary permittivity (bottom set of lines) against frequency throughout water uptake experiment for Prime20 cured at 60ºC, aged at 50ºC - where the legend indicates the time intervals the samples had been removed from the water.

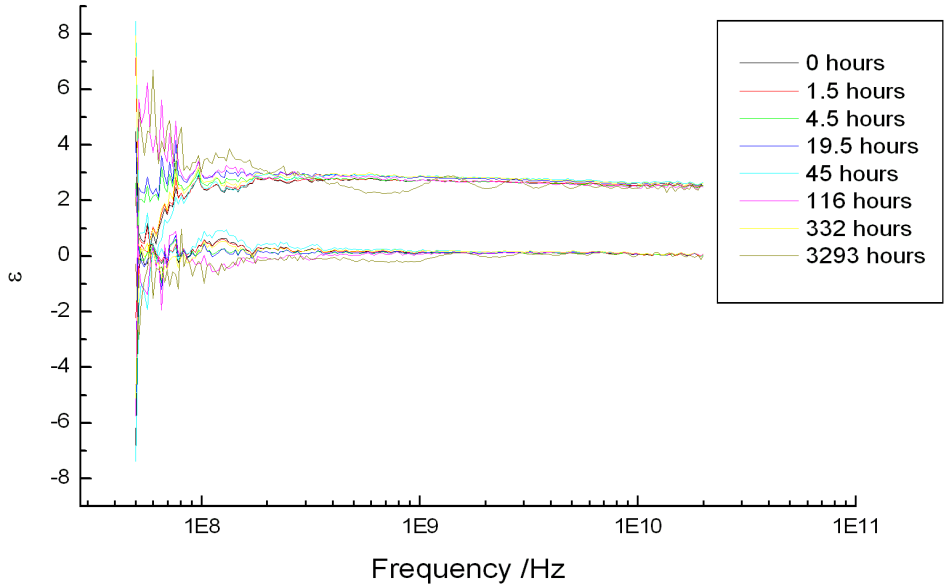

Figure 66. Changes in real permittivity (top set of lines) and imaginary permittivity (bottom set of lines) against frequency throughout water uptake experiment for Prime20 cured at 70ºC, aged at 50ºC - where the legend indicates the time intervals the samples had been removed from the water.

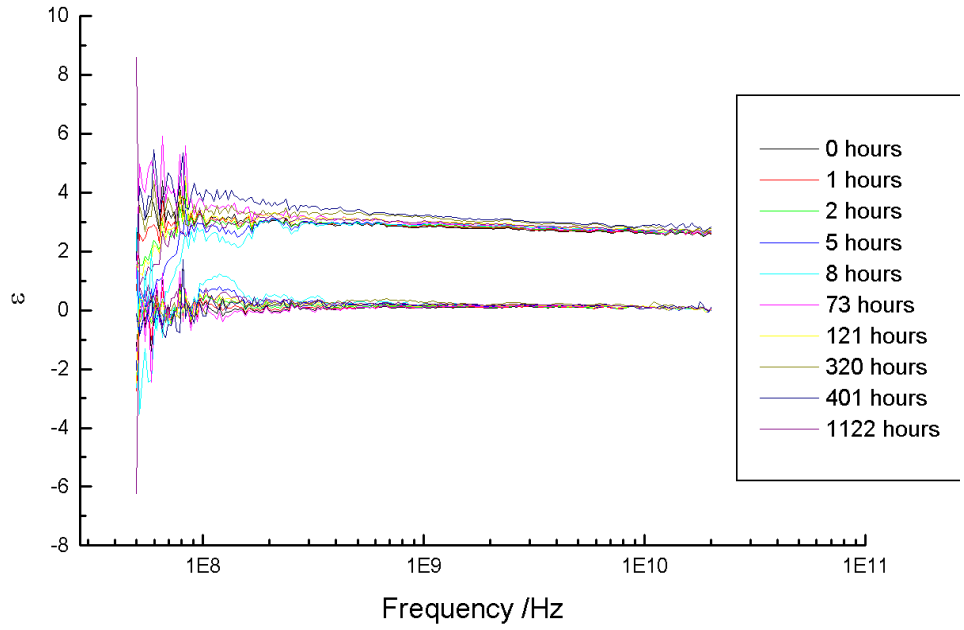

Figure 67. Changes in real permittivity (top set of lines) and imaginary permittivity (bottom set of lines) against frequency throughout water uptake experiment for Prime20 cured at 50ºC, aged at 70ºC - where the legend indicates the time intervals the samples had been removed from the water.

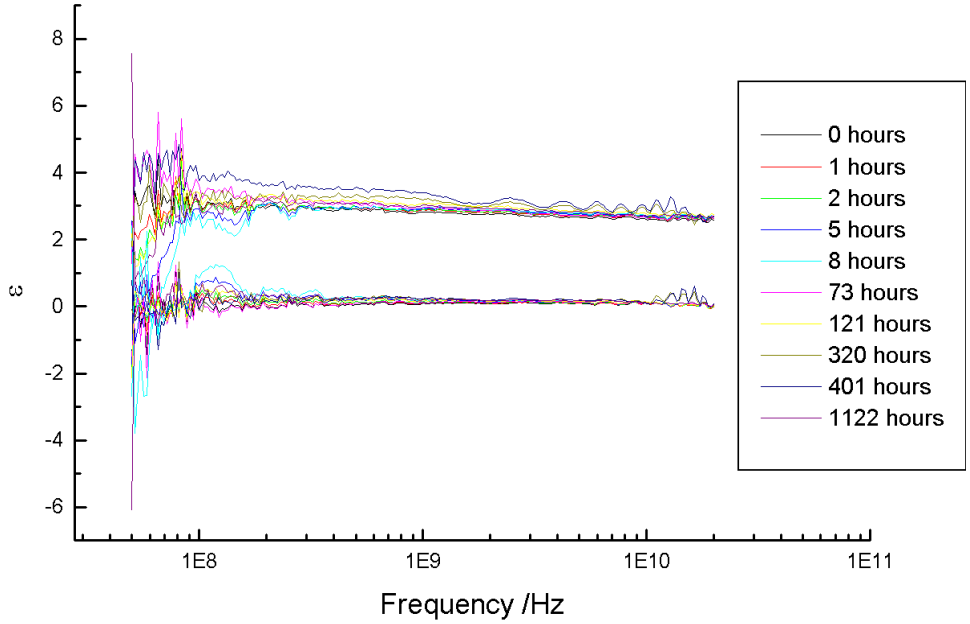

Figure 68. Changes in real permittivity (top set of lines) and imaginary permittivity (bottom set of lines) against frequency throughout water uptake experiment for Prime20 cured at 60ºC, aged at 70ºC - where the legend indicates the time intervals the samples had been removed from the water.

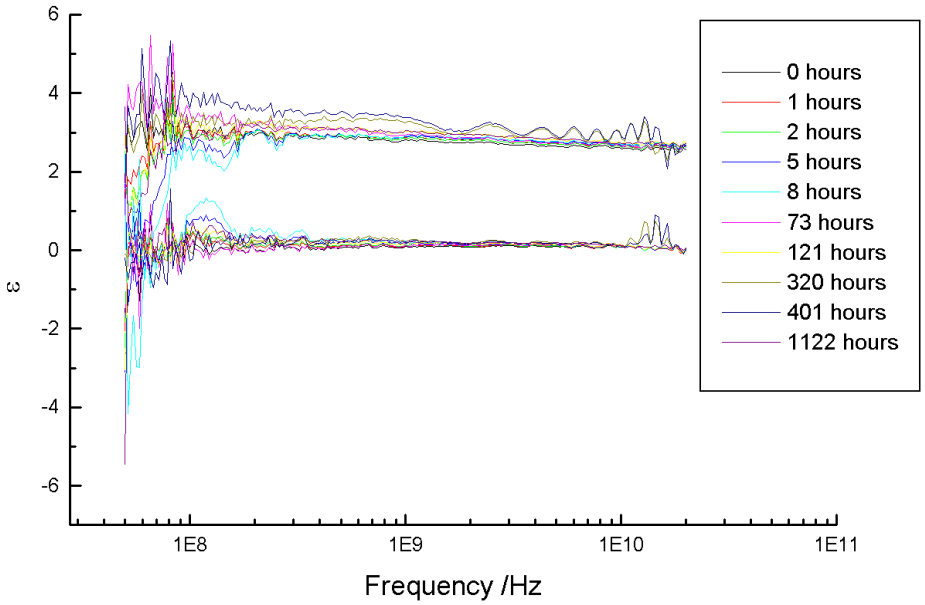

Figure 69. Changes in real permittivity (top set of lines) and imaginary permittivity (bottom set of lines) against frequency throughout water uptake experiment for Prime20 cured and aged at 70ºC - where the legend indicates the time intervals the samples had been removed from the water.

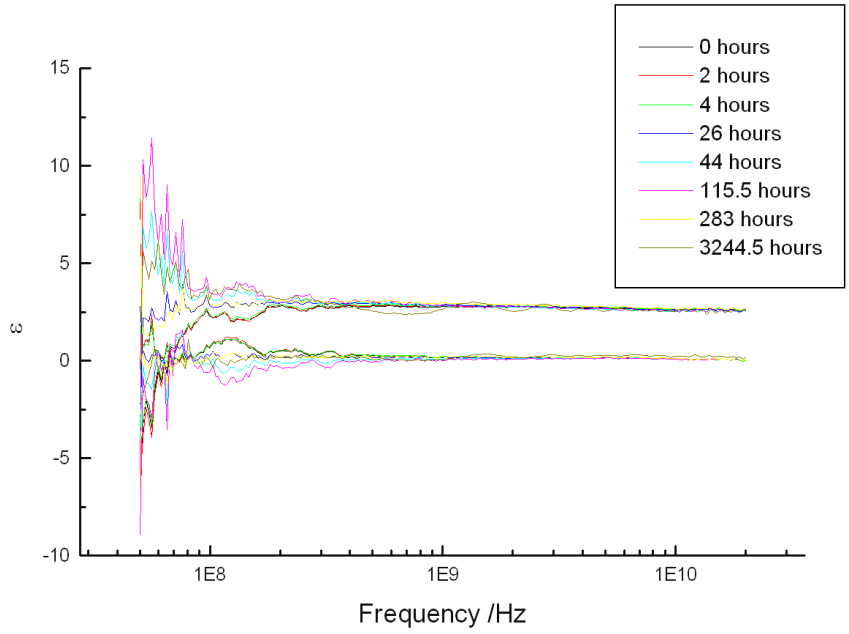

Figure 70. Changes in real permittivity (top set of lines) and imaginary permittivity (bottom set of lines) against frequency throughout water uptake experiment for the shared model system cured and aged at 50ºC - where the legend indicates the time intervals the samples had been removed from the water.

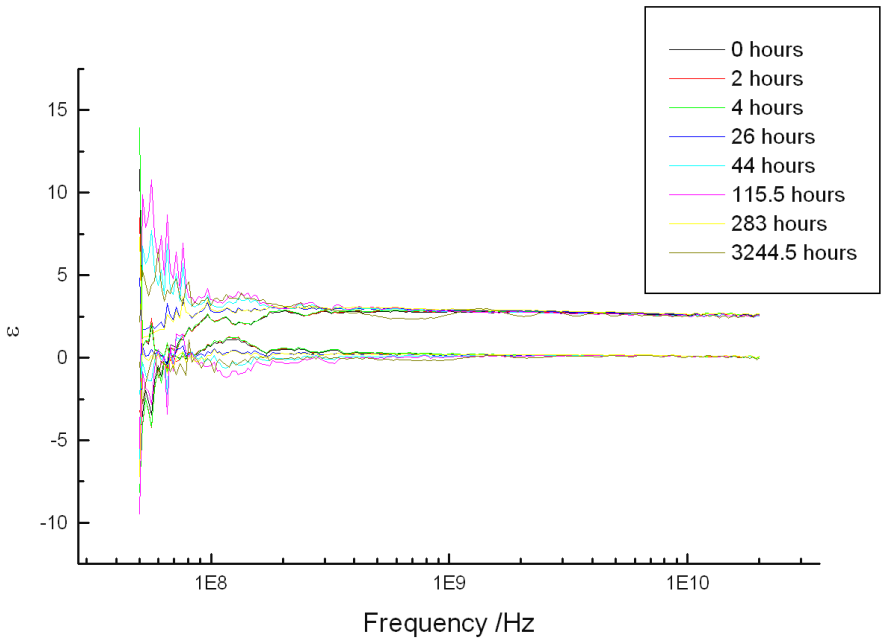

Figure 71. Changes in real permittivity (top set of lines) and imaginary permittivity (bottom set of lines) against frequency throughout water uptake experiment for the shared model system cured at 60ºC, aged at 50ºC - where the legend indicates the time intervals the samples had been removed from the water.

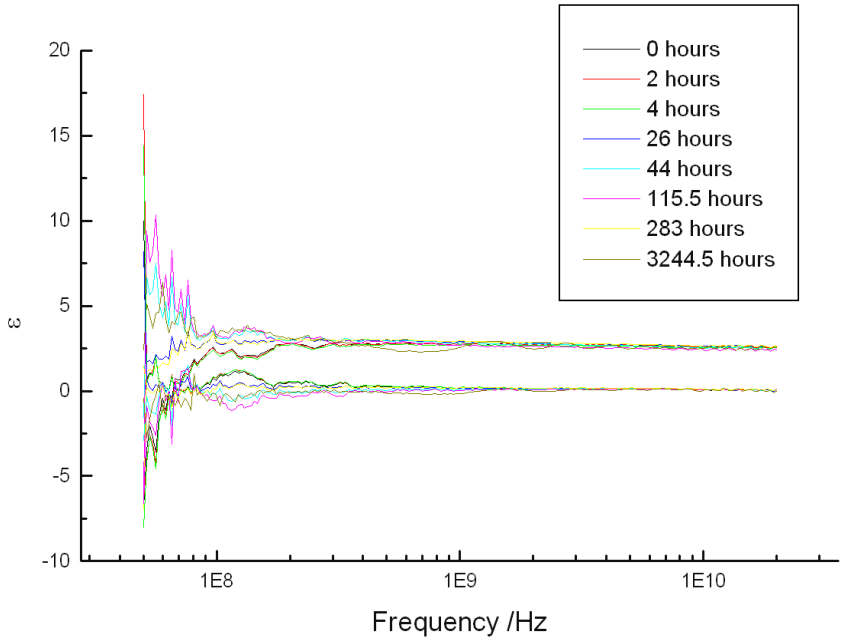

Figure 72. Changes in real permittivity (top set of lines) and imaginary permittivity (bottom set of lines) against frequency throughout water uptake experiment for the shared model system cured at 70ºC, aged at 50ºC - where the legend indicates the time intervals the samples had been removed from the water.

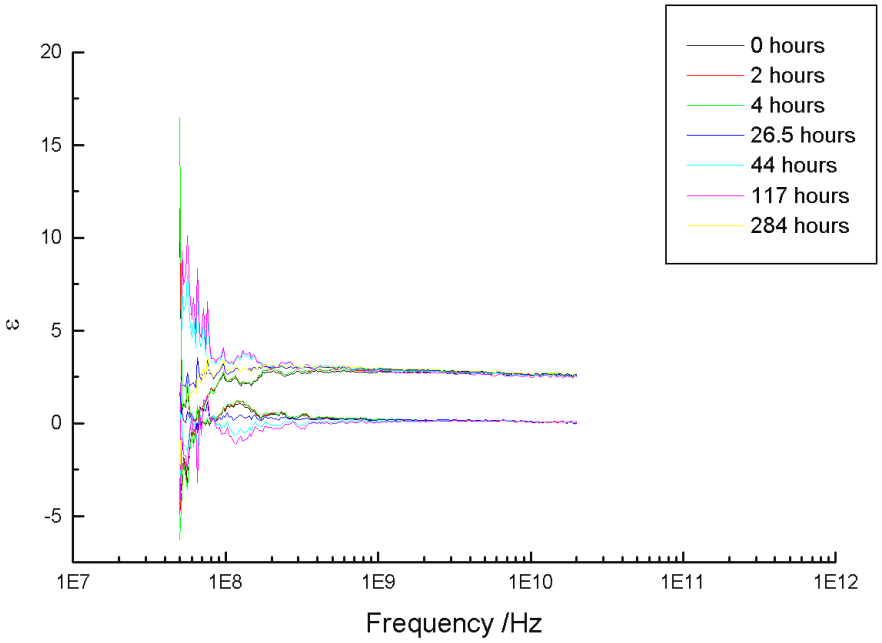

Figure 73. Changes in real permittivity (top set of lines) and imaginary permittivity (bottom set of lines) against frequency throughout water uptake experiment for the shared model system cured at 50ºC, aged at 70ºC - where the legend indicates the time intervals the samples had been removed from the water.

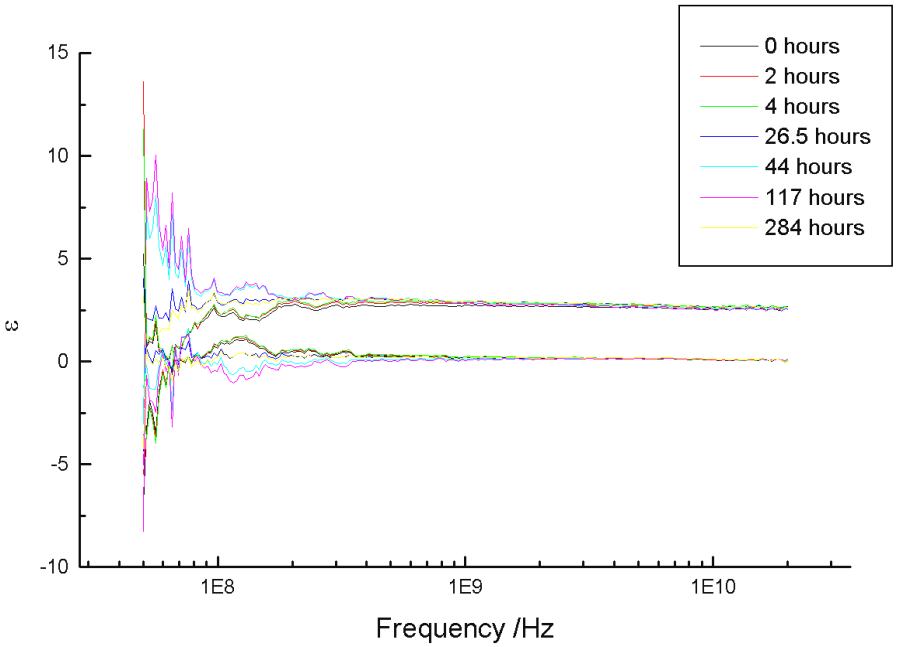

Figure 74. Changes in real permittivity (top set of lines) and imaginary permittivity (bottom set of lines) against frequency throughout water uptake experiment for the shared model system cured at 60ºC, aged at 70ºC - where the legend indicates the time intervals the samples had been removed from the water.

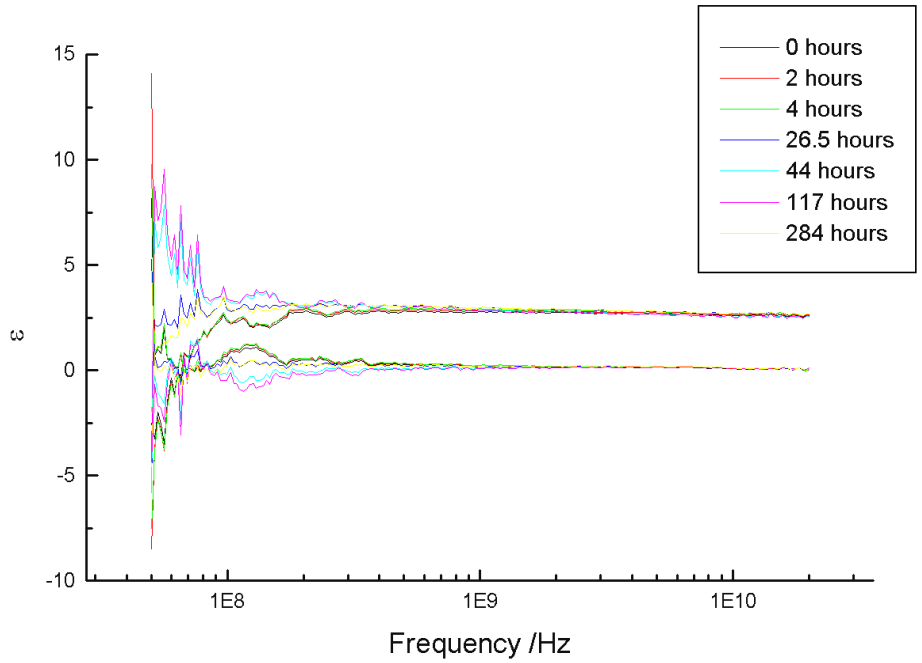

Figure 75. Changes in real permittivity (top set of lines) and imaginary permittivity (bottom set of lines) against frequency throughout water uptake experiment for the shared model system cured and aged at 70ºC - where the legend indicates the time intervals the samples had been removed from the water.

Water Ingress Mid Frequency Dielectric Plots

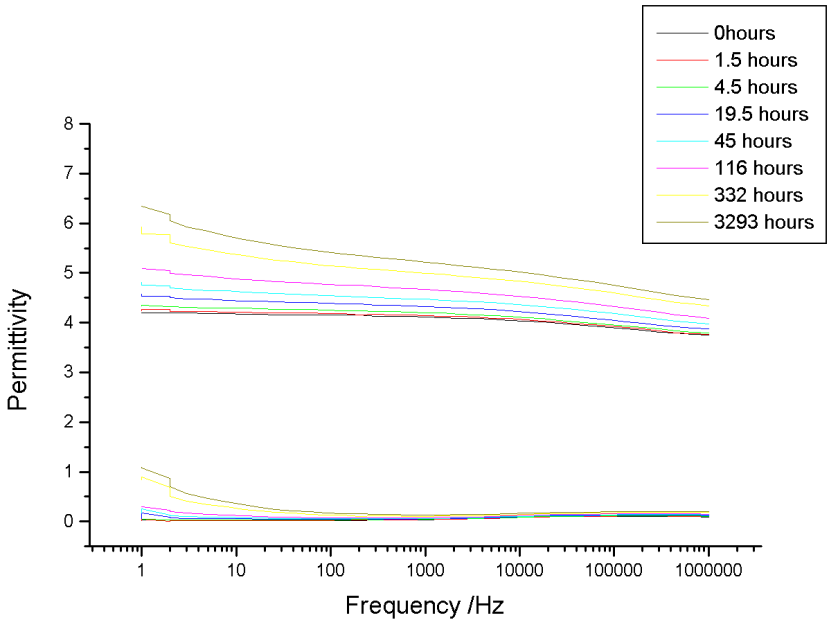

Figure 76. Changes in real permittivity (top set of lines) and imaginary permittivity (bottom set of lines) against frequency throughout water uptake experiment for Prime20 cured at 60ºC, aged at 50ºC - where the legend indicates the time intervals the samples had been removed from the water.

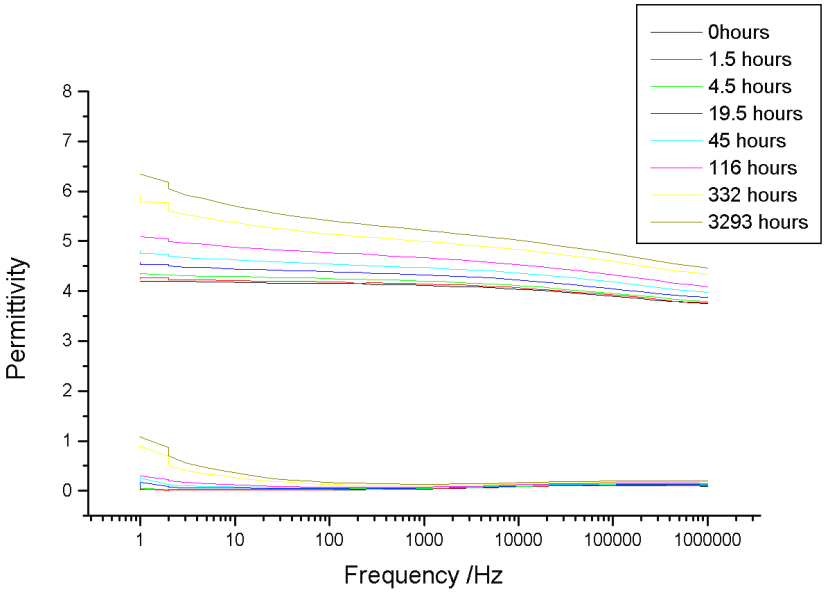

Figure 77. Changes in real permittivity (top set of lines) and imaginary permittivity (bottom set of lines) against frequency throughout water uptake experiment for Prime20 cured at 70ºC, aged at 50ºC - where the legend indicates the time intervals the samples had been removed from the water.

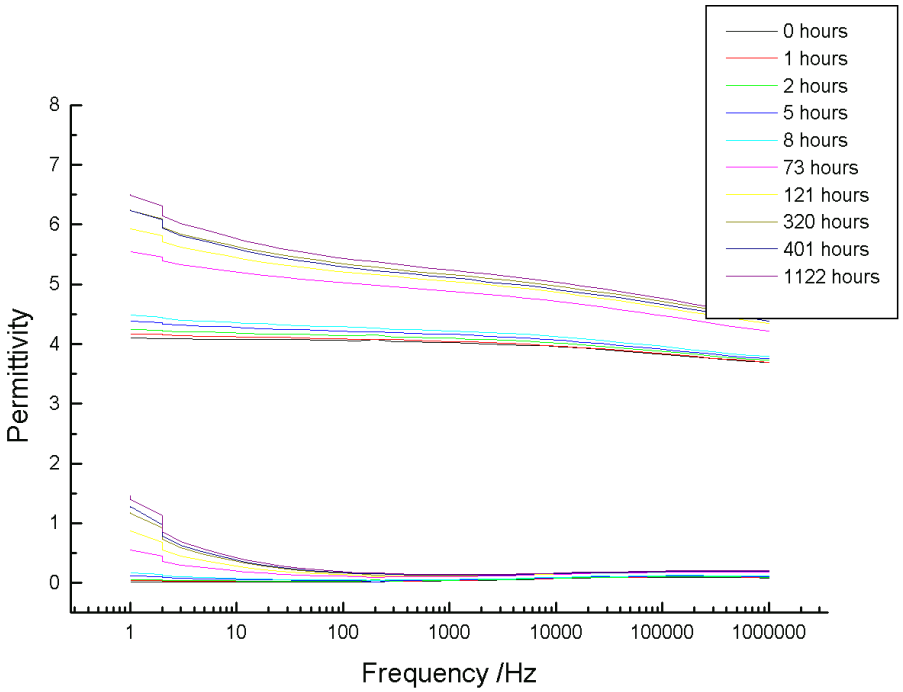

Figure 78. Changes in real permittivity (top set of lines) and imaginary permittivity (bottom set of lines) against frequency throughout water uptake experiment for Prime20 cured at 60ºC, aged at 70ºC - where the legend indicates the time intervals the samples had been removed from the water.

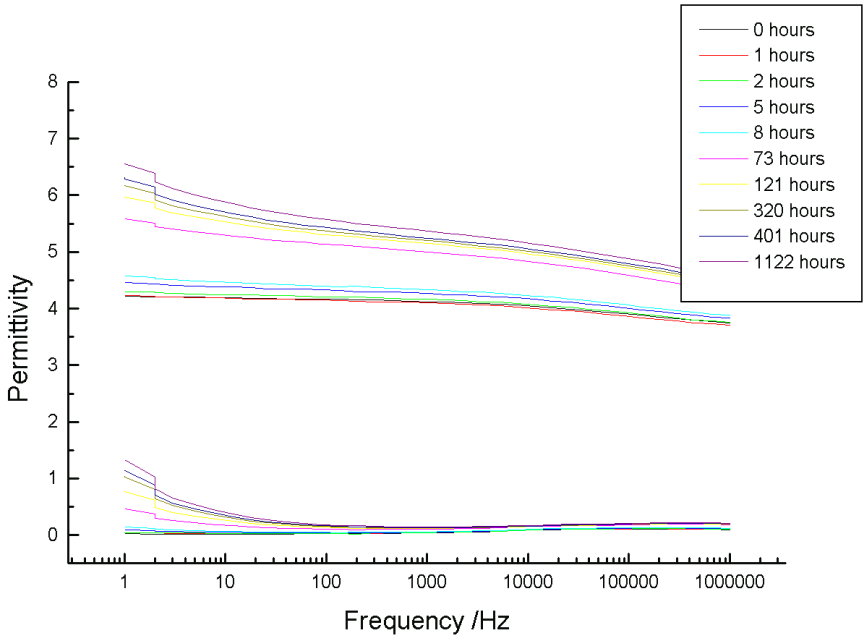

Figure 79. Changes in real permittivity (top set of lines) and imaginary permittivity (bottom set of lines) against frequency throughout water uptake experiment for Prime20 cured at 70ºC, aged at 70ºC - where the legend indicates the time intervals the samples had been removed from the water.

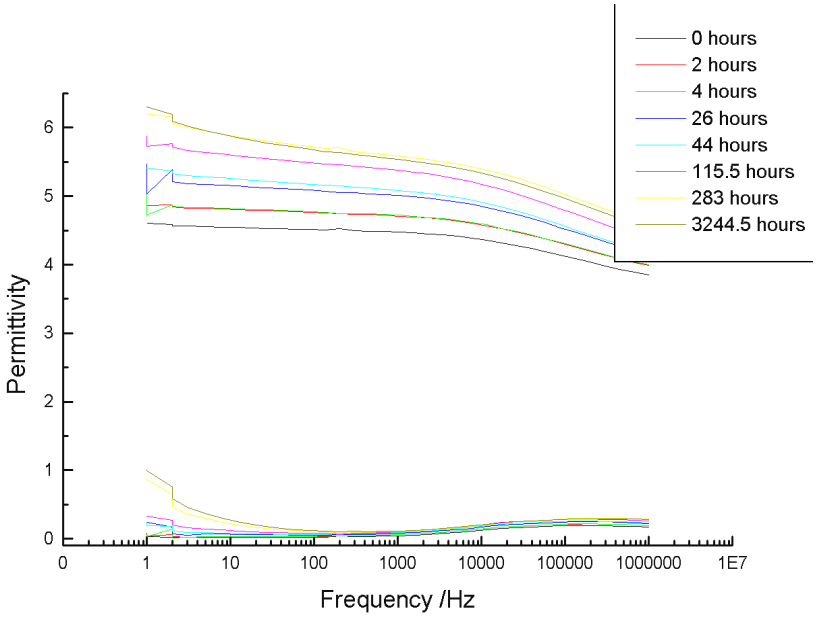

Figure 80. Changes in real permittivity (top set of lines) and imaginary permittivity (bottom set of lines) against frequency throughout water uptake experiment for the shared model system cured at 60ºC, aged at 50ºC - where the legend indicates the time intervals the samples had been removed from the water.

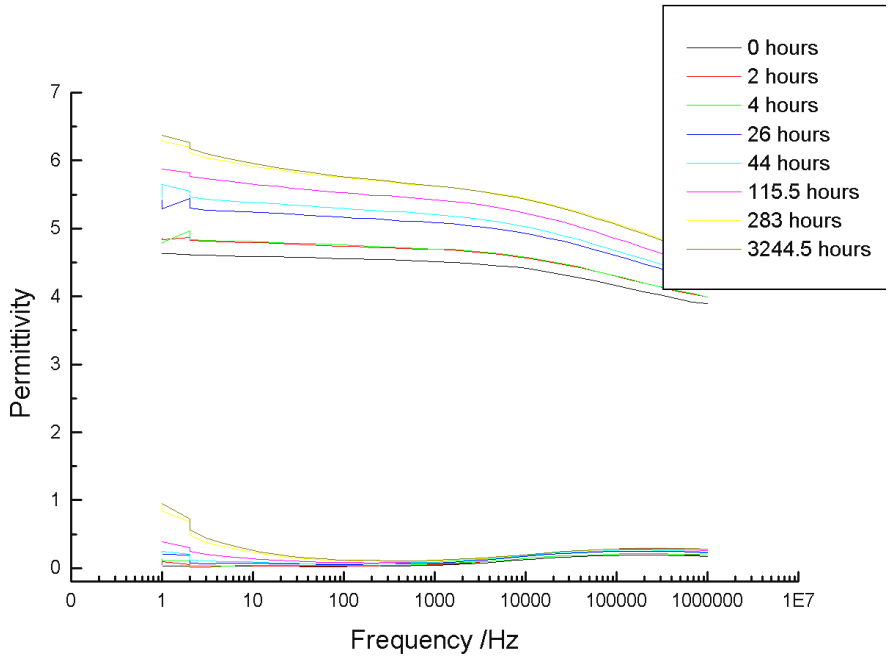

Figure 81. Changes in real permittivity (top set of lines) and imaginary permittivity (bottom set of lines) against frequency throughout water uptake experiment for the shared model system cured at 70ºC, aged at 50ºC - where the legend indicates the time intervals the samples had been removed from the water.

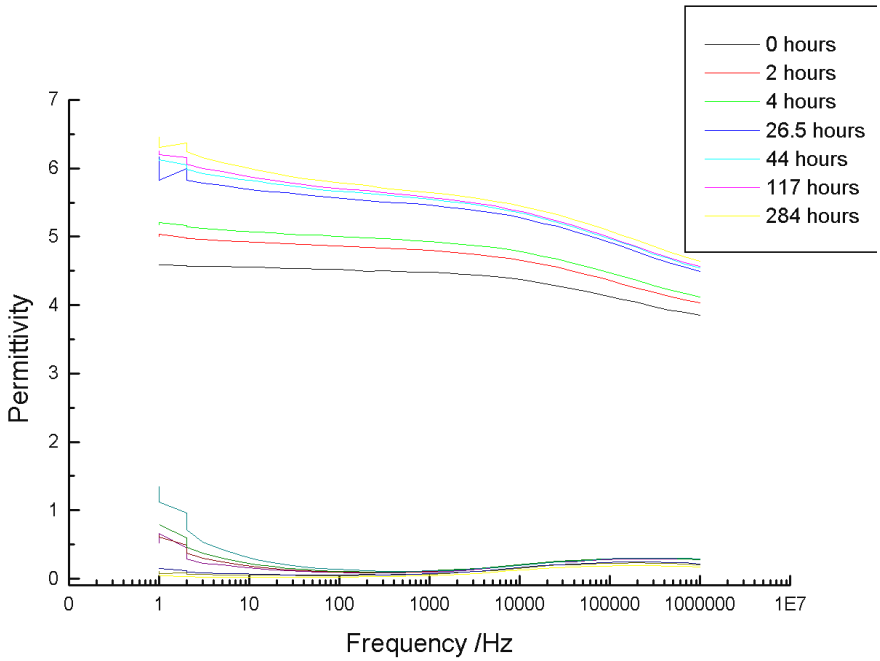

Figure 82. Changes in real permittivity (top set of lines) and imaginary permittivity (bottom set of lines) against frequency throughout water uptake experiment for the shared model system cured at 60ºC, aged at 70ºC - where the legend indicates the time intervals the samples had been removed from the water.

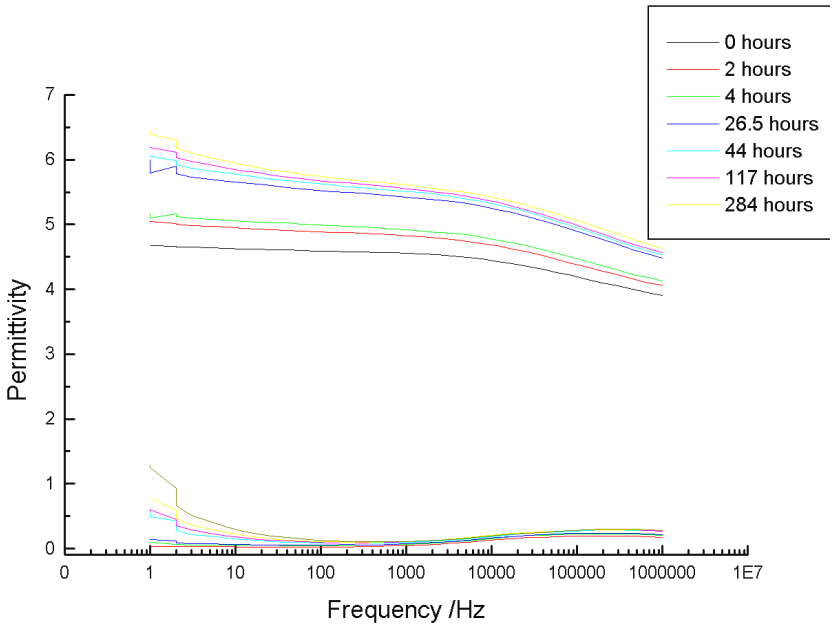

Figure 83. Changes in real permittivity (top set of lines) and imaginary permittivity (bottom set of lines) against frequency throughout water uptake experiment for the shared model system cured at 70ºC, aged at 70ºC - where the legend indicates the time intervals the samples had been removed from the water.